SAPIENZA
UNIVERSITÀ DI ROMA

TITOLO TESI

Facoltà di Medicina e Psicologia
Laurea Magistrale in Medicina e Chirurgia

Nome Cognome
ID number MATRICOLA

Relatrice
Dott.ssa Nome Cognome

Academic Year 2022/2023

Thesis defended on 24 Gennaio 2024
in front of a Board of Examiners composed by:

Prof. Tizio (chairman)

Prof. Caio

Prof. Sempronio

Prof. ...

Prof. ...

TITOLO TESI
Tesi sperimentale retrospettiva monocentrica. Sapienza University of Rome

This thesis has been typeset by LaTeX and the Sapthesis class.

Author's email: email autore

Abstract

Contesto

Obbiettivi

Metodi

Risultati

Contents

List of Figures

List of Tables

Chapter 1

Introduction

1.1 Previous Works

In the context of S&R[1] operations, the support of robots has become more and more extensive in recent years [24],[9] and in particular the necessity and advantages of using *decentralized multi-agent* systems [15]. A particular field of S&R missions focuses on high mountain scenarios, in which UAVs [2] are tasked with localizing avalanche victims. These missions involve the smart collaboration between UAVs and humans, developed also in the context of European founded projects such as the SHERPA one [13].

Different types of sensors can be used to achieve the localization goal, but the fastest and most accurate ones are electromagnetic sensors, which can operate also in noisy environments [20]. Among these, the ARTVAs[3] are the most commonly used in both human-conducted and robot-conducted operations.

Many studies have analyzed and formulated strategies and algorithms in the particular context of S&R operations using UAVs for avalanche victims [33], [29], [32]. Furthermore, in order to address the localization problem, the authors of [7] and [6] propose a robocentric SLAM approach in the broader robotics context. Note that in [7] they also take into consideration the *multiple victims* case.

Avalanche victims rescue missions are particularly difficult with respect to other S&R operations because of some challenging aspects. In particular, the time constraint is quite demanding since the survival chances of avalanche victims diminish rapidly with time. Victims buried under avalanches have a 93% survival rate within the first 15 minutes, which drops to 25% after 45 minutes due to hypothermia [2] and plateaus at 21% from 60 min to 180 minutes [30].

The common human-conducted avalanche victims S&R technique using ARTVA technology relies on three phases. In the first phase, rescuers search for the first valid electromagnetic signal, which can be detected at distances ranging from 20 meters for single-antenna receiver to 80 meters for triple-antenna ones. In the second phase, rescuers are trained to interpret the magnetic field data and follow standard procedures in order to follow magnetic field direction and find the victim's position. In the final phase, rescuers dig to save the buried individual.

[1] S&R stands for Search and Rescue.

[2] UAV stands for Unmanned Aerial Vehicles.

[3] ARTVA stands for the Italian "Apparecchio di Ricerca dei Travolti in VAlanga".

Despite the effectiveness of this technique, it requires a significant amount of time due to the challenges of traversing avalanche terrain. Additionally, rescuers walking on unstable snow face the tangible risk of triggering a secondary avalanche [6]. For these reasons, and given the additional advantage of typically not encountering obstacles in high mountain scenarios, the use of intelligent *autonomous* drones results in a faster and safer search when compared to human rescuers, as shown in [18], [22], [21].

Therefore, the aim of this work is to build upon previous efforts to *automate* and improve the efficiency of the second phase by developing a mathematical/algorithmic framework for solving the localization problem of not just one, but *multiple avalanche victims*, using *multiple decentralized* agents (UAVs). This approach aims to reduce computational complexity without sacrificing accuracy and convergence time.

1.2 The ARTVA

The ARTVA technology is composed of two different and easy switchable modalities: in *receiver* mode, the instrument senses and processes the electromagnetic field emitted by the ARTVA *transmitter* (carried by the avalanche victim).

The magnetic field generated by the solenoid antenna of the instrument oscillates with a frequency of 457 kHz and its characteristics are defined in the standard ETS 300 718-1 [31], to ensure compatibility between different brands and models. To save batteries and facilitate detection, the magnetic field is transmitted in pulses of a tenth of a second every second [6].

As will be discussed more in-depth in the following chapter, the magnetic field can be modeled as a three-dimensional vector field, which means that it assigns a certain intensity and direction to each point in space. Therefore, the main difference between different kinds of ARTVAs lies in *"how much"* of this field they can measure. According to this criterion, the instruments can be divided into three different types [6]:

- ARTVAs *with one reception antenna*: the oldest models, usually analog. The same antenna is used in both *transmitter* and *receiver* mode. Therefore, only the projection of the magnetic field on the antenna can be measured. This type of ARTVA is the most difficult to use and the most time-consuming one.
- ARTVAs *with two perpendicular reception antennas*: are based on digital technology such as microprocessors. This type can measure only the intensity and direction of the horizontal component of the field, only when held in horizontal position.
- ARTVAs *with three mutually perpendicular reception antennas*: also based on digital technology. Since these ARTVAs possess three perpendicular antennas, they can measure the complete vector field. For this reason, the instrument can be oriented w.r.t the magnetic field in any way.

In this work, we will consider only new ARTVA transceivers (three antennas), which can achieve a search strip width in digital mode of 80 m and a maximum range in analog mode of 90 m [36]. Furthermore, it is important to point the transceiver in the direction of the avalanche, parallel to the slope. For this reason, in this work, two different types of trajectories have been considered.

1.3 Gradient, Divergence, and Curl

We briefly define the following operators which will be used throughout this work.

1.3.1 Gradient of a Scalar Field

Definition

Given a scalar function $f(x_1, x_2, \ldots, x_n) : \mathbb{R}^n \to \mathbb{R}$ or scalar field, the gradient of the function is a vector field of partial derivatives and denoted by ∇f, is defined as:

$$\nabla f = \left(\frac{\partial f}{\partial x_1}, \frac{\partial f}{\partial x_2}, \frac{\partial f}{\partial x_3}, \ldots, \frac{\partial f}{\partial x_n} \right) \tag{1.1}$$

where ∇ is the vector differential operator [14].

Properties

The gradient is a vector which points in the direction of the greatest ascent of the function and its magnitude is the increase.

1.3.2 Definition of a Vector Field

A **vector field** on a subset $S \subseteq \mathbb{R}^n$ is a vector-valued function $\mathbf{V} : S \to \mathbb{R}^n$ that assigns to each point $\mathbf{x} = (x_1, x_2, \ldots, x_n) \in S$ a vector $\mathbf{V}(\mathbf{x})$ [14].

1.3.3 Divergence of a Vector Field

For simplicity and since we are working with $\mathbb{R}^3$ Euclidean space, we limit our discussion from now on to Euclidean coordinates.

Definition

Given a vector field $\mathbf{V}$, the divergence of $\mathbf{V}$ at a point $\mathbf{p} \in \mathbb{R}^3$ is defined as the net outward flux of $\mathbf{V}$ per unit volume Δv as the volume about the point tends to zero:

$$\nabla \cdot \mathbf{V} = \lim_{\Delta v \to 0} \frac{1}{\Delta v} \iint_S \mathbf{V} \cdot d\mathbf{s} \tag{1.2}$$

where $\mathbf{V} \cdot d\mathbf{s}$ is the flux of $\mathbf{V}$ through the surface S [16].

Since $\mathbf{V} = V_x \mathbf{e_x} + V_y \mathbf{e_y} + V_z \mathbf{e_z}$, the divergence of $\mathbf{V}$, can be computed as:

$$\nabla \cdot \mathbf{V} = \frac{\partial V_x}{\partial x} + \frac{\partial V_y}{\partial y} + \frac{\partial V_z}{\partial z} \tag{1.3}$$

where V_x, V_y, and V_z are the components of the vector field $\mathbf{V}$ in the x, y, and z directions, respectively [14].

Properties

When the vector field is represented using flux lines (indicating the direction and intensity), the divergence is the amount of flux lines diverging/converging through a given point.

A net outward flux of a vector field through a surface bounding a volume indicates the presence of a source, the divergence measures the strength of the source. The divergence of a vector field is a scalar field.

1.3.4 Laplacian of a Vector Field

The Laplacian of a vector field $\mathbf{V}$, denoted by ∇^2, is similar to the scalar Laplacian and is defined as:

$$\nabla^2 V = \frac{\partial^2 V_x}{\partial x^2} + \frac{\partial^2 V_y}{\partial y^2} + \frac{\partial^2 V_z}{\partial z^2} \tag{1.4}$$

Alternatively, by taking the curl of the curl of a vector field, the Laplacian can be expressed as:

$$\nabla^2 \mathbf{V} = \nabla(\nabla \cdot \mathbf{V}) - \nabla \times (\nabla \times \mathbf{V}) \tag{1.5}$$

1.3.5 Curl of a Vector Field

Definition

The curl of $\mathbf{V}$, denoted by $\nabla \times \mathbf{V}$, at a point in space $\mathbf{x} \in \mathbb{R}^3$ is a vector field whose magnitude is the maximum net circulation of $\mathbf{V}$ per unit area as the area tends to zero and whose direction is the normal direction of the area when the area is oriented to make the net circulation maximum:

$$\nabla \times \mathbf{V} = \lim_{\Delta s \to 0} \frac{1}{\Delta s} \mathbf{n} \oint_C \mathbf{V} \cdot d\mathbf{l} \tag{1.6}$$

where $\mathbf{n}$ is the unit normal vector to the surface S, $d\mathbf{l}$ is the differential line element along the boundary, and the integral represents the circulation of $\mathbf{V}$ around the boundary of the surface [16].

The curl of a vector field $\mathbf{V}$ can be then computed in terms of its components [14]:

$$\nabla \times \mathbf{V} = \left(\frac{\partial V_z}{\partial y} - \frac{\partial V_y}{\partial z}, \frac{\partial V_x}{\partial z} - \frac{\partial V_z}{\partial x}, \frac{\partial V_y}{\partial x} - \frac{\partial V_x}{\partial y} \right) \tag{1.7}$$

Properties

Since the normal to an area can point in two opposite directions, the direction of the curl is given by the right-hand rule. A vortex source causes a circulation of the vector field around it. The circulation of a vector field around a closed path is defined as the scalar line integral of the vector over the path. Note that a circulation of $\mathbf{V}$ can exist even when the divergence of $\mathbf{V}$ is zero, meaning there is no net source or sink.

1.4 Stokes' Theorem

The surface integral of the curl of a vector field $\mathbf{V}$ over a surface s is equal to the line integral of the vector field over the boundary contour c of the surface:

$$\oint_C \mathbf{V} \cdot d\mathbf{l} = \iint_S (\nabla \times \mathbf{V}) \cdot d\mathbf{s} \tag{1.8}$$

The proof of the theorem comes directly from the definition of the curl 1.6 and by dividing the surface S into smaller areas. The idea comes from the fact that computing the line integral around the boundary of a surface is equal to compute the integral for all the smaller areas, since the $d\mathbf{l}$ components of the neighbouring regions are in opposite directions.

1.5 Divergence Theorem

The theorem states that the surface integral of a vector field $\mathbf{V}$ over a closed surface S is equal to the volume integral of the divergence of $\mathbf{V}$ over the volume enclosed by S:

$$\iint_S \mathbf{V} \cdot d\mathbf{s} = \iiint_V (\nabla \cdot \mathbf{V})\, dv \tag{1.9}$$

The idea of the proof is similar to 1.4, starting from the definition of the divergence 1.2. Considering a volume divided into smaller volumes, the contributions from the internal surfaces cancel each other, leaving only the contribution from the outer surface.

1.6 Null Identity Theorem

The divergence of the curl of any vector field is always zero [16]:

$$\nabla \cdot (\nabla \times \mathbf{V}) = 0 \tag{1.10}$$

The proof leverages the divergence theorem 1.9 applied to the vector field $\nabla \cdot (\nabla \times \mathbf{V})$. Considering that any volume can be divided in half, then the surface bounding the volume would be the sum of 2 surfaces, connected by a common boundary that has been drawn twice. One can then compute the two surface integrals using 1.8, and since the two normals $\mathbf{n}$ have equal intensity and opposite direction, their sum is zero and the integrand as well.

A converse statement of the theorem is as follows: If a vector field $\mathbf{B}$ is divergence-less, then it can be expressed as the curl of another vector field $\mathbf{V}$:

$$\nabla \cdot \mathbf{B} = 0 \implies \mathbf{B} = \nabla \times \mathbf{V}$$

Since the identity $\nabla \cdot (\nabla \times \mathbf{V}) = 0$ always holds, it means that for any magnetic field $\mathbf{B}$ with zero divergence, we can find a vector potential $\mathbf{V}$ such that $\mathbf{B}$ is the curl of $\mathbf{V}$.

1.7 Phasor Notation

For dealing with time-varying vector fields, we use phasor notation to represent sinusoidal varying field vectors (which is usually the case in real-world applications, such as the magnetic dipole) [16]. Phasor notation simplifies the analysis of such fields by converting differential equations into algebraic equations.

Then, an harmonic vector field $\mathbf{V}(x, y, z, t) = \mathbf{V}(x, y, z)\, \cos \omega t$ can be represented by a vector phasor that depends on space coordinates but not on time:

$$\mathbf{V}(x, y, z, t) = \mathbf{V}(x, y, z) e^{j\omega t}$$

where ω is the angular frequency and $\mathbf{V}(x, y, z)$ is a vector phasor that contains information on direction, magnitude, and phase.

The time-domain function can be recovered from the phasor by taking the real part:

$$\mathbf{V}(x, y, z, t) = \mathrm{Re}\{\mathbf{V}(x, y, z) e^{j\omega t}\}$$

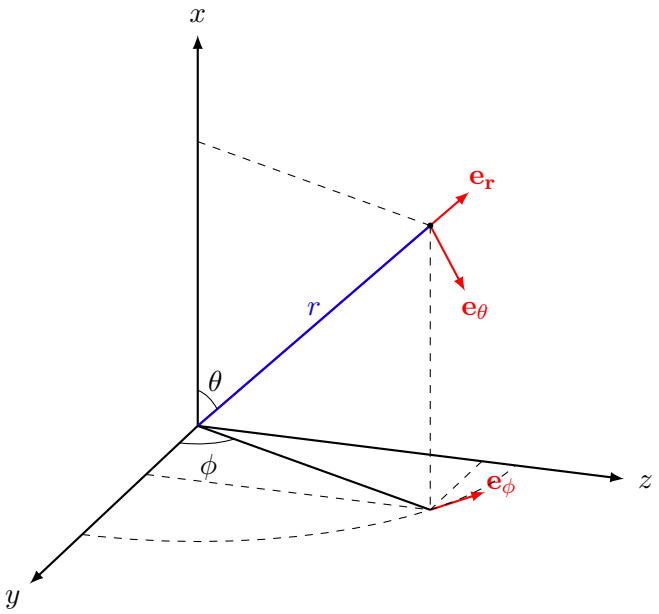

Figure 1.1 Spherical and Cartesian coordinates with their respective unit vectors.

1.8 Spherical Coordinates

We define two classical coordinate systems: spherical coordinates (r, θ, ϕ) and Cartesian coordinates (x, y, z), with their respective vector basis $\{\mathbf{e}_r, \mathbf{e}_\theta, \mathbf{e}_\phi\}$ and $\{\mathbf{e}_x, \mathbf{e}_y, \mathbf{e}_z\}$, represented in Figure 1.1, from which the following relationships are evident. Note that we use the convention in [33] for the angles and the axes.

1.8.1 Conversion from Cartesian to Spherical Coordinates

$$r = \sqrt{x^2 + y^2 + z^2}, \tag{1.11}$$

$$\theta = \cos^{-1}\left(\frac{\sqrt{z^2 + y^2}}{x}\right), \tag{1.12}$$

$$\phi = \tan^{-1}\left(\frac{y}{z}\right). \tag{1.13}$$

1.8.2 Conversion from Cartesian to Spherical Coordinates

$$x = r\cos\theta, \tag{1.14}$$

$$y = r\sin\theta\cos\phi, \tag{1.15}$$

$$z = r\sin\theta\sin\phi. \tag{1.16}$$

1.8.3 Expressing Spherical Unit Vectors using Cartesian Unit Vectors

A point $\mathbf{r}$ in Cartesian coordinates is given by:

$$\mathbf{r} = x\,\mathbf{e}_x + y\,\mathbf{e}_y + z\,\mathbf{e}_z.$$

The radial unit vector $\mathbf{e}_r$ is defined as the normalized position vector, obtained by substituting the coordinates in 1.8.1:

$$\mathbf{e}_r = \frac{\mathbf{r}}{|\mathbf{r}|} = \cos\theta\,\mathbf{e}_x + \sin\theta\cos\phi\,\mathbf{e}_y + \sin\theta\sin\phi\,\mathbf{e}_z. \tag{1.17}$$

The unit vector $\mathbf{e}_\theta$, which is perpendicular to $\mathbf{e}_r$ and lies in the plane formed by the origin and the z-axis, points in the direction of increasing θ. It can be found by taking the partial derivative of the position vector with respect to θ and normalize it:

$$\mathbf{e}_\theta = -\sin\theta\,\mathbf{e}_x + \cos\theta\cos\phi\,\mathbf{e}_y + \cos\theta\sin\phi\,\mathbf{e}_z. \tag{1.18}$$

Similarly, the unit vector $\mathbf{e}_\phi$, which is perpendicular to both $\mathbf{e}_r$ and $\mathbf{e}_\theta$, points in the direction of increasing ϕ. It can be derived by taking the partial derivative of the position vector with respect to ϕ and normalize it:

$$\mathbf{e}_\phi = \frac{\frac{\partial \mathbf{r}}{\partial \phi}}{|\frac{\partial \mathbf{r}}{\partial \phi}|} = -\sin\phi\,\mathbf{e}_y + \cos\phi\,\mathbf{e}_z.$$

1.8.4 The Gradient, Divergence, and Curl in Spherical Coordinates

We omit the demonstration of how these formulas are found starting from the definitions given in Cartesian coordinates 1.3, which involve large amount of computations [16].

For a vector field expressed in spherical coordinates:

$$\mathbf{V} = V_r\mathbf{e}_R + V_\theta\mathbf{e}_\theta + V_\phi\mathbf{e}_\phi$$

the divergence is:

$$\nabla\cdot\mathbf{V} = \frac{1}{r^2}\frac{\partial}{\partial r}(r^2V_r) + \frac{1}{r\sin\theta}\frac{\partial}{\partial\theta}(\sin\theta V_\theta) + \frac{1}{r\sin\theta}\frac{\partial V_\phi}{\partial\phi}. \tag{1.19}$$

The curl in spherical coordinates is:

$$\nabla\times\mathbf{V} = \frac{1}{r\sin\theta}\begin{vmatrix} \mathbf{e}_r & r\mathbf{e}_\theta & r\sin\theta\mathbf{e}_\phi \\ \frac{\partial}{\partial r} & \frac{\partial}{\partial\theta} & \frac{\partial}{\partial\phi} \\ V_r & rV_\theta & r\sin\theta V_\phi \end{vmatrix}. \tag{1.20}$$

carrying out the determinant:

$$\begin{aligned}\nabla\times\mathbf{V} = \frac{1}{r\sin\theta}\Bigg[&\left(\frac{\partial}{\partial\theta}(V_\phi\sin\theta) - \frac{\partial V_\theta}{\partial\phi}\right)\mathbf{e}_r \\ &+ \left(\frac{1}{\sin\theta}\frac{\partial V_r}{\partial\phi} - \frac{\partial}{\partial r}(rV_\phi)\right)\mathbf{e}_\theta \\ &+ \left(\frac{\partial}{\partial r}(rV_\theta) - \frac{\partial V_r}{\partial\theta}\right)\mathbf{e}_\phi\Bigg].\end{aligned} \tag{1.21}$$

1.9 3D Dirac Delta

Definition

Given a point $\mathbf{r}$ in Cartesian coordinates, the Dirac delta function $\delta(\mathbf{r})$ is defined as [17]:

- $\delta(\mathbf{r}) = 0$ at all points except at $\mathbf{r} = (0, 0, 0)$.
- The integral across the entire space satisfies:

$$\int_V \delta(\mathbf{r})\, dv = 1 \tag{1.22}$$

The result of the integral could be the value of any function in zero, $f(0)$. For example, the Dirac delta could be the charge density ρ 2.1 of a point particle located at the origin whose charge is q.

1.10 Green's Function for Poisson Equation

Poisson's equation using Green's function is written as:

$$\nabla^2 G(\mathbf{r}) = \delta(\mathbf{r}) \tag{1.23}$$

The solution to the above equation is given by:

$$G(r) = -\frac{1}{4\pi r}$$

Proof

We assume $G(r)$ to be axis-symmetric, implying that it only depends on the magnitude r, not the vector position $\mathbf{r}$. Considering the point (x, y, z) and the distance r from the origin. To find Green function we look for the simplest function that satisfies the equation, which has the form:

$$G(r) = A\frac{1}{r} + B$$

where A and B are constants.

Assuming $B = 0$ for simplicity, we find A by integrating over a sphere of volume ϵ. Substituting Poisson's equation 1.23 in the the definition of the Dirac delta 1.22:

$$\int_V \nabla^2 G(r)\, dv = 1$$

Using the divergence theorem 1.9:

$$\int_V \nabla^2 G(r)\, dv = \int_S \nabla G(r) \cdot d\mathbf{s}$$

$$1 = \int_S \nabla G(r) \cdot d\mathbf{s}$$

The right-hand side represents the flux through the surface S. We take the integral over the surface of a sphere of radius r, knowing that the surface area is $4\pi r^2$ and computing the divergence (which is just the derivative thanks to the assumption) of $A\,\frac{1}{r}$:

$$1 = \int_S -\frac{A}{r^2} d\mathbf{s} = -\frac{4\pi\eta^2 A}{\eta^2}$$

From which we conclude:

$$A = -\frac{1}{4\pi}$$

Chapter 2

Electromagnetism

The ARTVA instrument in transmitter and receiver mode is a magnetic dipole. In order to formulate a coherent mathematical model, it is necessary to report some results of electromagnetic theory. Firstly, we identify and name the fundamental electromagnetic physical quantities.

Symbol	Description	Units
$\mathbf{E}$	Electric field intensity	V/m
$\mathbf{D}$	Electric displacement field	C/m^2
$\mathbf{H}$	Magnetic field intensity	A/m
$\mathbf{B}$	Magnetic flux density	T
$\mathbf{J}$	Current density	A/m^2
$\mathbf{A}$	Magnetic vector potential	V $\cdot$ s/m
$\mathbf{m}$	Magnetic vector moment	A $\cdot$ m^2
ρ	Volume charge density	C/m^3
ϵ	Permittivity of the medium	F/m
μ	Permeability of the medium	H/m
c	Speed of light in vacuum	m/s

Table 2.1 List of electromagnetic physical quantities and their descriptions.

2.1 Maxwell's Equations

We postulate Maxwell's equations in a simple (linear, isotropic, and homogeneous) medium in phasor notation 1.7, which have been discovered experimentally [16]:

$$\nabla \times \mathbf{E} = -j\omega\mathbf{B} \tag{2.1}$$
$$\nabla \times \mathbf{H} = \mathbf{J} + j\omega\epsilon\mathbf{E} \tag{2.2}$$
$$\nabla \cdot \mathbf{E} = \frac{\rho}{\epsilon} \tag{2.3}$$
$$\nabla \cdot \mathbf{B} = 0 \tag{2.4}$$

In these equations, the space-coordinate arguments have been omitted for simplicity. The fact that the same notations are used for the phasors as are used for their corresponding time-dependent quantities should create little confusion because we will deal exclusively with sinusoidal vector fields.

From Maxwell's equation 2.4, we know that the magnetic flux density $\mathbf{B}$ is solenoidal (zero divergence). Then, $\mathbf{B}$ can be expressed as the curl of another vector field using the Null Theorem 1.10, obtaining 2.4:

$$\mathbf{B} = \nabla \times \mathbf{A} \tag{2.5}$$

Also, $\mathbf{B}$ relates to the magnetic field intensity $\mathbf{H}$ through the permeability of the medium μ:

$$\mathbf{B} = \mu\mathbf{H} \tag{2.6}$$

Another useful form of Maxwell's first equation 2.1 can be found by substituting 2.5:

$$\nabla \times \mathbf{E} = -j\omega(\nabla \times \mathbf{A}) = -\nabla \times j\omega\mathbf{A}$$
$$\nabla \times (\mathbf{E} + j\omega\mathbf{A}) = 0$$

Since the sum of vector fields is itself a vector field, $\mathbf{E} + j\omega\mathbf{A}$ is a vector field, and we can define a **scalar** field, the electric potential V, such that:

$$\mathbf{E} + j\omega\mathbf{A} = -\nabla V \tag{2.7}$$

If the curl of a vector field is zero, a scalar field exists whose gradient gives the vector field.

2.1.1 Conservation of Charge Principle

The principle of conservation of charge states that the net charge within a closed system remains constant over time, meaning no charge can be created nor destroyed [16]:

$$\nabla \cdot \mathbf{J} = -\frac{\partial\rho}{\partial t} \tag{2.8}$$

The current density $\mathbf{J}$ is defined as:

$$\mathbf{J} = Nq\mathbf{u} \tag{2.9}$$

where N is the number of charge carriers per unit volume, q is the charge of each carrier, and $\mathbf{u}$ is the drift velocity of the charge carriers.

This means that if a current flows out of a volume, the charge density inside the volume must decrease at a rate equal to the current. The current leaving the volume is the flux of the current density through surface S:

$$I = \oint_S \mathbf{J} \cdot d\mathbf{s} \tag{2.10}$$

2.2 Wave Equation for Magnetic Vector Potential

In order to determine the intensity of the magnetic field, we first need to find an expression for the magnetic vector potential $\mathbf{A}$, called the wave equation. Starting from Maxwell's equations, we find the wave equation by substituting 2.5 and 2.6 into the second Maxwell equation 2.2:

$$\nabla \times \nabla \times \mathbf{A} = \mu\mathbf{J} + j\omega\epsilon\mu\mathbf{E}$$

Then we substitute 2.7 for $\mathbf{E}$ and use the Laplacian 1.5 on the left side:

$$\nabla(\nabla \cdot \mathbf{A}) - \nabla^2\mathbf{A} = \mu\mathbf{J} + j\omega\epsilon\mu\left(-\nabla V - j\omega\mathbf{A}\right)$$

The definition of a vector requires the specification of both its curl and its divergence. Although the curl of $\mathbf{A}$ is designated $\mathbf{B}$ in 2.5, we are still at liberty to choose its divergence to simplify the expression [16]:

$$\nabla \cdot \mathbf{A} = -j\omega\epsilon\mu V$$

Finally, rearranging the terms and substituting the square of j, we get:

$$\nabla^2\mathbf{A} + \omega^2\epsilon\mu\mathbf{A} = -\mu\mathbf{J}$$

This is the wave equation for the magnetic vector potential $\mathbf{A}$:

$$\nabla^2\mathbf{A} - k^2\mathbf{A} = -\mu\mathbf{J} \tag{2.11}$$

where $k = \omega\sqrt{\mu\epsilon}$ is the wave number, which characterizes the propagation of the electromagnetic wave in the medium.

2.2.1 Finding the Potential by Solving the Wave Equation

Since both $\mathbf{A}$ and $\mathbf{J}$ are vector fields, the wave equation 2.11 can be written for each component of $\mathbf{A}$:

$$\nabla^2 \begin{pmatrix} A_x \\ A_y \\ A_z \end{pmatrix} = k^2 \begin{pmatrix} A_x \\ A_y \\ A_z \end{pmatrix} - \mu \begin{pmatrix} J_x \\ J_y \\ J_z \end{pmatrix} \tag{2.12}$$

In order to solve 2.12, we can use the Green function for Poisson's equation 1.23 for each of the components when $k = 0$ (the case of static fields). Then, the solution is given by the formula:

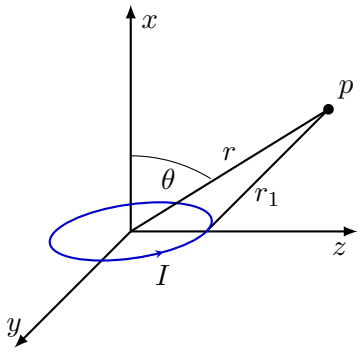

Figure 2.1 Magnetic dipole representation

$$\mathbf{A} = \frac{\mu}{4\pi} \int_V \mathbf{J} \frac{e^{-jkr}}{r} dv \tag{2.13}$$

by using the superposition principle and by finding the solution of the time-dependent differential equation.

2.3 Magnetic Dipole

We have a small filament loop of radius b, carrying an AC current $I(t) = I\cos(\omega t)$ as shown in Figure 2.1. If S is the cross-section area of the wire and dl a differential length, we have $\mathbf{J} \perp \mathbf{s}$, the normal to the area and the volume:

$$dv = S\, dl \tag{2.14}$$

In order to determine the magnetic field intensity $\mathbf{H}$ at a certain point in space p, we need to compute the magnetic vector potential $\mathbf{A}$ first [16]. Since the charges move only in the thin wire, they are located only in the wire region, then from the definition of current 2.10:

$$I = S\,\mathbf{J}$$

The volume integral in 2.13 becomes:

$$\int_V \mathbf{J}\, dv = \int_V \mathbf{J}\, S\, dl$$

Then, we substitute 2.10 and change the integral type since it is now the sum over the length, so the formula becomes (the current must flow in a closed path):

$$\mathbf{A} = \frac{\mu_0 I}{4\pi} \oint_C \frac{d\mathbf{l}}{r_1} e^{-jkr_1} \tag{2.15}$$

where r_1 is the distance between the point p and the charges (source element) and $d\mathbf{l}$ is a vector tangent to the loop of differential length dl.

Assumption

We can then simplify 2.15 by considering the radius b to be small enough, such that $r_1 - r \approx 0$. Then by adding and subtracting r from the power of the exponential:

$$e^{-jkr_1} = e^{-jk(r_1+r-r)} = e^{-jkr}\, e^{-jk(r_1-r)}$$

Then by using Taylor approximation on the second exponential ($x = r_1 - r \approx 0$) we obtain:

$$e^{-jkr_1} = e^{-jkr}\, [1 - jk(r_1 - r)]$$

Then, we substitute this result in 2.15 and simplify:

$$\begin{aligned}\mathbf{A} &= \frac{\mu_0 I}{4\pi} e^{-jkr}\, [1 - jk(r_1 - r)] \oint_C \frac{d\mathbf{l}}{r_1} \\ &= \frac{\mu_0 I}{4\pi} e^{-jkr} \left(\oint \frac{d\mathbf{l}}{r_1} - jk \oint (r_1 - r) \frac{d\mathbf{l}}{R_1} \right)\end{aligned}$$

Since the integral of $d\mathbf{l}$ over a closed loop is zero, because we have considered a small loop $b \to 0$:

$$\oint_C d\ell = 2\pi b \quad \to \quad \oint_C d\ell \to 0$$

Then we obtain:

$$\mathbf{A} = \frac{\mu_0 I}{4\pi} e^{-jkr} \left[(1 + jkr) \oint \frac{d\mathbf{l}}{r_1} \right] \tag{2.16}$$

Assumption Quasi-Static Field/Near Field Zone

If we consider a region near the magnetic dipole, we obtain quasi-static fields. We defined the wave number k as:

$$k = \omega\sqrt{\mu\epsilon} \tag{2.17}$$

Electromagnetic waves propagate with velocity u (speed of light in vacuum) [16]:

$$u = \frac{1}{\sqrt{\mu\epsilon}} \tag{2.18}$$

Then, by inverting 2.18 and substituting in 2.17, we can write k as:

$$k = \frac{\omega}{u} \tag{2.19}$$

From wave theory $f = \frac{\omega}{2\pi}$ and $\lambda = \frac{u}{f}$, we obtain another expression for u:

$$u = \frac{\lambda\, \omega}{2\, \pi} \tag{2.20}$$

Therefore, we can substitute 2.3 in 2.19:

$$k = \frac{2\pi}{\lambda} \tag{2.21}$$

To simplify the expression for $\mathbf{A}$ 2.15, we make the assumption that $k\,r \ll 1$, and if we substitute the found expression of k 2.21:

$$k\,r \ll 1 \implies \frac{2\pi r}{\lambda} \ll 1 \implies r \ll \frac{\lambda}{2\pi}$$

This means that r needs to be small in comparison to λ. If this is the case:

$$e^{-jkr} \approx e^{0} = 1$$

We eliminate completely the time dependence and obtain the expression for $\mathbf{A}$:

$$\mathbf{A} = \frac{\mu_0 I}{4\pi} \oint_C \frac{d\mathbf{l}}{r_1} \tag{2.22}$$

In the ARTVA case, the standard operating frequency is $f = 475\,\text{kHz}$ and the optimal range of the instrument is $< 80\,\text{m}$. Then in the worst case, when $r = 80\,\text{m}$, we obtain the approximation $k\,r = 0.79$.

Symmetry

In the particular case of a magnetic dipole, the magnetic vector potential $\mathbf{A}$ is symmetric with respect to the x-axis, therefore independent to the ϕ angle 1.8. This is true since we can choose freely the z-axis and y-axis orientation in space around the loop. Then we can choose the point $\mathbf{p}$ to lie on the zx-plane or the yx-plane; in both cases, we will obtain that one of the two $d\mathbf{l}$ components $d\mathbf{l_z}$ and $d\mathbf{l_y}$ will cancel themselves out as we integrate over the loop.

For example, if we consider the point to lie on the yx-plane, then take a point on the loop where $d\mathbf{l}$ is and its symmetric w.r.t. the y-axis, the component $d\mathbf{l_y}$ of the first will cancel itself out with the one of the second.

We can write the length of a circumference as $l = r\,\alpha$, where α is the subtended angle by the length l and r the radius. In addition, we express $\mathbf{e}_\phi$ using the Cartesian basis:

$$\mathbf{e}_\phi = -\sin\phi\,\mathbf{e_y} + \cos\phi\,\mathbf{e_z}$$

Then, $d\mathbf{l}$ magnitude depends on the differential angle $d\phi$ and the radius b, and has the same direction as $\mathbf{e}_\phi$:

$$d\mathbf{l} = b\,d\phi\,\mathbf{e}_\phi = b\,d\phi\,(-\sin\phi\,\mathbf{e_y} + \cos\phi\,\mathbf{e_z}) \tag{2.23}$$

For every $d\mathbf{l}$, there is another symmetrically located differential length element on the other side of the y-axis that will contribute an equal amount to $\mathbf{A}$ in the $\mathbf{e_z}$ direction but will cancel the contribution of $d\mathbf{l}$ in the $\mathbf{e_y}$ direction. Since $\mathbf{e_z} = \mathbf{e}_\phi$, if point P lies on the yx-plane, equation 2.22 can be written as:

$$\mathbf{A} = \mathbf{e}_\phi \frac{\mu I b}{4\pi} \int_0^{2\pi} \frac{\cos\phi}{r_1}\,d\phi \tag{2.24}$$

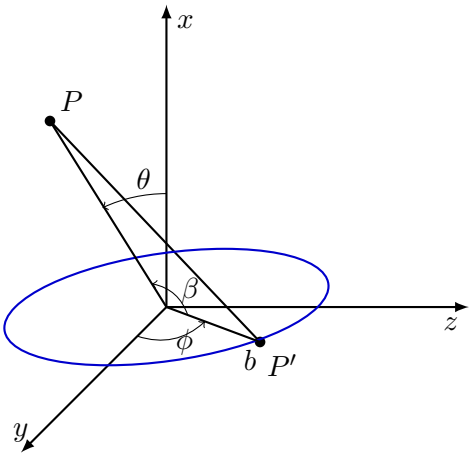

Figure 2.2 Magnetic dipole representation with the OPP' triangle

Computing the Integral in Spherical Coordinates

Firstly, we find r_1 by applying the law of cosines on the triangle OPP', Figure 2.2:
We start with the equation for r_1:

$$r_1^2 = r^2 + b^2 - 2rb\cos\beta$$

Since we are on the xy-plane, we can write the $\mathbf{b}$ and $\mathbf{r}$ vectors as:

$$\mathbf{r} = r\sin\theta\,\mathbf{e_y} + r\cos\theta\,\mathbf{e_x}$$

$$\mathbf{b} = b\cos\phi\,\mathbf{e_y} + b\sin\phi\,\mathbf{e_z}$$

Then we find the angle β between $\mathbf{r}$ and $\mathbf{b}$:

$$\cos\beta = \frac{\mathbf{b}\cdot\mathbf{r}}{rb} = \sin\theta\cos\phi$$

We have obtained a formula for r_1:

$$r_1 = \sqrt{r^2 + b^2 - 2rb\sin\theta\cos\phi}$$

Simplifying further, we get:

$$r_1^2 = r^2\left(1 + \frac{b^2}{r^2} - 2\,\frac{b}{r}\sin\theta\cos\phi\right)$$

Using the same assumption as before, that the loop is very small with respect to r (i.e., $b \ll r$ and therefore $b^2 \ll r^2$), we can write:

$$r_1 \approx r\left(1 - 2\,\frac{b}{r}\,\sin\theta\cos\phi\right)^{1/2}$$

Then we compute the inverse $\frac{1}{r_1}$ and use the Taylor approximation to the first derivative, considering $x = 2\,\frac{b}{r}\,\sin\theta\cos\phi$, which tends to zero, we obtain:

$$\frac{1}{r_1} \approx \frac{1}{r}\left(1 + \frac{b}{r}\sin\theta\cos\phi\right) \tag{2.25}$$

Now, substituting 2.25 in 2.24, we can calculate the integral for $\mathbf{A}$ over the entire loop:

$$\mathbf{A} = \mathbf{e}_\phi \frac{\mu I b}{4\pi}\int_0^{2\pi}\left(1 + \frac{b}{r}\sin\theta\cos\phi\right)\cos\phi\, d\phi$$

Since b, r, and θ do not depend on ϕ, the first integral is zero, and the second one gives π:

(1) $$\int_0^{2\pi}\cos\phi\, d\phi = \sin\phi\Big|_0^{2\pi} = 0$$

(2) $$\int_0^{2\pi}\cos^2\phi\, d\phi = \int_0^{2\pi}\frac{1+\cos(2\phi)}{2}\, d\phi = \frac{1}{2}\cdot 2\pi + \frac{1}{2}\cdot 0 = \pi$$

Therefore, we obtain:

$$\mathbf{A} = \mathbf{e}_\phi \frac{\mu I b^2}{4\, r^2}\sin\theta \tag{2.26}$$

Magnetic Field Intensity H

Finally, we can now obtain an expression in spherical coordinates of the magnetic field intensity $\mathbf{H}$, by first finding $\mathbf{B}$ using 2.5 and then inverting 2.6.
We compute the curl of $\mathbf{A}$ in spherical coordinates 1.20:

$$\mathbf{B} = \nabla\times\mathbf{A} = \frac{1}{r^2\sin\theta}\begin{vmatrix} \mathbf{e_r} & \mathbf{e}_\theta r & \mathbf{e}_\phi r\sin\theta \\ \frac{\partial}{\partial r} & \frac{\partial}{\partial\theta} & \frac{\partial}{\partial\phi} \\ 0 & 0 & r\sin\theta A_\phi \end{vmatrix} =$$

$$= \frac{1}{r^2\sin\theta}\left(\mathbf{e_r}\frac{\partial}{\partial\theta}(r\sin\theta A_\phi) - \mathbf{e}_\theta\frac{\partial}{\partial r}(r\sin\theta A_\phi)\right)$$

where A_ϕ is the magnitude of the vector field found in 2.26, while A_r and A_θ are zero since the potential has only the $\mathbf{e}_\phi$ direction. Substituting 2.26:

$$\mathbf{B} = \frac{1}{r^2\sin\theta}\frac{\mu b^2 I}{4\pi}\left(\mathbf{e_r}\frac{2}{r}\cos\theta\sin\theta + \mathbf{e}_\theta r\sin^2\theta\, r^{-2}\right) =$$
$$= \frac{\mu I b^2}{4\, r^3}\left(\mathbf{e_r}2\cos\theta + \mathbf{e}_\theta\sin\theta\right)$$

Then, by inverting equation 2.6, we obtain the final expression for $\mathbf{H}$:

$$\mathbf{H} = \frac{I b^2}{4\, r^3}\left(\mathbf{e_r}2\cos\theta + \mathbf{e}_\theta\sin\theta\right) \tag{2.27}$$

which can also be expressed using the Cartesian unit vectors $(\mathbf{e}_x, \mathbf{e}_y, \mathbf{e}_z)$ by substituting $\mathbf{e}_r$ with 1.17 and $\mathbf{e}_\theta$ with 1.18:

$$\mathbf{H} = \frac{Ib^2}{4\pi\, r^3}\left[(2\cos^2\theta - \sin^2\theta)\mathbf{e}_x + 3\cos\theta\sin\theta\cos\phi\,\mathbf{e}_y + 3\cos\theta\sin\theta\sin\phi\,\mathbf{e}_z\right]$$

or in vector form:

$$\mathbf{H} = \frac{Ib^2}{4\,r^3}\begin{bmatrix} 2\cos^2\theta - \sin^2\theta \\ 3\cos\theta\sin\theta\cos\phi \\ 3\cos\theta\sin\theta\sin\phi \end{bmatrix}$$

We can finally find the expression for $\mathbf{H}$ using only Cartesian coordinates by inverting the equations in 1.8.2:

$$\mathbf{H} = \frac{Ib^2}{4\,r^5}\begin{bmatrix} 2x^2 - y^2 - z^2 \\ 3xy \\ 3xz \end{bmatrix} \tag{2.28}$$

This expression has been derived by applying the Pythagorean identity.

2.4 Normalized Source Strength

The magnetic field intensity $\mathbf{H}$ and the magnetic flux density $\mathbf{B}$ are vector fields sensible to the orientation of the source coordinate system. The expression for $\mathbf{H}$, as given in equation 2.28, is expressed with respect to a coordinate system centered at the center of the current loop, as we have seen in the previous section. However, we need to introduce a quantity which is invariant with respect to the orientation of the electromagnetic target. Many studies have conducted in-depth analysis on rotational invariants of the magnetic gradient tensor, such as [23] and [38]. The magnetic gradient tensor is simply the transposed Jacobian of the magnetic flux density $\mathbf{B}$, and it is defined as follows:

$$\begin{aligned}\mathbf{G} &= \begin{bmatrix} \frac{\partial B_x}{\partial x} & \frac{\partial B_y}{\partial x} & \frac{\partial B_z}{\partial x} \\ \frac{\partial B_x}{\partial y} & \frac{\partial B_y}{\partial y} & \frac{\partial B_z}{\partial y} \\ \frac{\partial B_x}{\partial z} & \frac{\partial B_y}{\partial z} & \frac{\partial B_z}{\partial z} \end{bmatrix} \\ &= \begin{bmatrix} B_{xx} & B_{yx} & B_{zx} \\ B_{xy} & B_{yy} & B_{zy} \\ B_{xz} & B_{yz} & B_{zz} \end{bmatrix}\end{aligned} \tag{2.29}$$

It represents the spatial rate of change of the magnetic field vector $\mathbf{B}$ along the three mutually orthogonal directions of the Cartesian coordinates.

In most cases, rotational invariants, such as the Frobenius norm of $\mathbf{G}$ and any combination of its eigenvalues, are sensitive to the direction of the target magnetic moment vector $\mathbf{m}$ [37]. The magnetic moment represents the strenght and orientation of the magnetic field, and for a magnetic dipole of a current loop it is defined as follows, [16]:

$$\mathbf{m} = I\,\mathbf{S} \tag{2.30}$$

where I is the current flowing in the loop and $\mathbf{S}$, is the normal to the area of the loop and it is not to be confused with S in 2.14, which is the area of the section of the wire. In our representation of the magentic dipole, with the Cartesian axes defined in Figure 2.1, the direction of the magnetic moment is the x-axis, and the magnitude is:

$$m = I\,\pi\,b^2 \tag{2.31}$$

Instead the NSS[1], a tensor invariant calculated from the eigenvalues of the magnetic gradient tensor $\mathbf{G}$, does not depend on the magnetization direction and it is completely isotropic around the magnetic dipole [38]. This follows from the magnetic gradient tensor $\mathbf{G}$ being symmetric and traceless, thanks to Maxwell's equations.

In particular from the fourth equation 2.4, and from the definition of gradient 1.1 we deduce the traceless property:

$$\nabla \cdot \mathbf{B} = 0 \Rightarrow \frac{\partial B_x}{\partial x} + \frac{\partial B_y}{\partial y} + \frac{\partial B_z}{\partial z} = 0 \Rightarrow B_{xx} + B_{yy} + B_{zz} = 0 \tag{2.32}$$

Instead, from the second Maxwell's equation (2.2), in the case of the quasi-static field assumption we used before, and considering regions of space where there is an absence of electric currents ($\mathbf{J} = 0$), the curl of $\mathbf{B}$ is zero ($\nabla \times \mathbf{B} = 0$), [12]. Then, from the definition of curl (1.7), we deduce the symmetry property:

$$\begin{aligned} \nabla \times \mathbf{B} = 0 \Rightarrow \frac{\partial B_x}{\partial y} - \frac{\partial B_y}{\partial x} = 0, \quad \frac{\partial B_x}{\partial z} - \frac{\partial B_z}{\partial x} = 0, \quad \frac{\partial B_y}{\partial z} - \frac{\partial B_z}{\partial y} = 0 \\ \Rightarrow B_{xy} = B_{yx}, \quad B_{xz} = B_{zx}, \quad B_{yz} = B_{zy} \end{aligned} \tag{2.33}$$

The NSS is a combination of the eigenvalues of the tensor $\mathbf{G}$. In order to find the eigenvectors of a matrix, we need to solve the equation:

$$\mathbf{G}\mathbf{v}_i = \lambda_i \mathbf{v}_i \tag{2.34}$$

which is true for all pairs of eigenvalue λ_i and eigenvector $\mathbf{v}_i$. The eigenvalues are found by solving the characteristic polynomial, defined as:

$$\det(\mathbf{G} - \lambda\mathbf{I}) = 0 \tag{2.35}$$

where $\mathbf{I}$ is the identity matrix. Expanding the determinant yields the cubic equation:

$$\lambda^3 - I_1\lambda^2 + I_2\lambda - I_3 = 0 \tag{2.36}$$

where I_1 is the trace of the gradient tensor $\mathbf{G}$, I_2 is the sum of the principal minors, and I_3 is the determinant of $\mathbf{G}$. However, since $\mathbf{G}$ is traceless, meaning that the coefficient of λ^2 vanishes, $I_1 = 0$, we can simplify the cubic equation as done in [12]:

$$\lambda^3 + I_2\lambda - I_3 = 0 \tag{2.37}$$

The invariants I_1, I_2, and I_3 are found following the linear algebra definitions mentioned before and simplified thanks to the symmetric property:

[1] NSS stands for Normalized Source Strength

1. I_1 (Trace):

$$I_1 = B_{xx} + B_{yy} + B_{zz} = 0$$

2. I_2 (Sum of principal minors):

$$\begin{aligned} I_2 &= B_{xx}B_{yy} + B_{yy}B_{zz} + B_{xx}B_{zz} - (B_{xy}B_{yx} + B_{yz}B_{zy} + B_{xz}B_{zx}) = \\ &= B_{xx}B_{yy} + B_{yy}B_{zz} + B_{xx}B_{zz} - (B_{xy}^2 + B_{yz}^2 + B_{xz}^2) \end{aligned}$$

3. I_3 (Determinant):

$$\begin{aligned} I_3 &= B_{xx}(B_{yy}B_{zz} - B_{zy}B_{yz}) - B_{yx}(B_{xy}B_{zz} - B_{zy}B_{xz}) + B_{zx}(B_{xy}B_{yz} - B_{yy}B_{xz}) = \\ &= B_{xx}B_{yy}B_{zz} + 2B_{xy}B_{yz}B_{xz} - B_{xx}B_{yz}^2 - B_{yy}B_{xz}^2 - B_{zz}B_{xy}^2 \end{aligned}$$

It is shown later in 2.4.1 that these coefficients are rotational invariants of the tensor $\mathbf{G}$, meaning that they are unchanged by a rotation of the coordinate axes. They have the neat property that they can be simply expressed directly in terms of the tensor components with respect to any Cartesian reference frame. Each distinct root of the cubic equation defines a corresponding eigenvalue of the tensor. From linear algebra we know that for each eigenvalue λ_i, the associated eigenvectors can be found as non-zero vectors $\mathbf{v}_i$ that satisfy 2.34. Also, since $\mathbf{G}$ is a symmetric real 3×3 matrix, all its eigenvalues are real, and the eigenvectors corresponding to distinct eigenvalues are orthogonal. It is always possible to construct an orthonormal set of the three eigenvectors, even in cases where the eigenvalues are degenerate (i.e., two or more eigenvalues are equal). Furthermore, it is demonstrated later in 2.4.1 that the eigenvalues λ_{min}, λ_{med}, and λ_{max} are rotational invariants of the tensor [12]. Therefore, any combination of the eigenvalues constitutes a rotational invariant and the NSS is defined as:

$$\text{NSS} = \sqrt{\lambda_{\text{med}}^2 - \lambda_{\text{min}}\lambda_{\text{max}}} \tag{2.38}$$

Additionally, it is shown that the NSS is inversely proportional to the fourth power of the distance between the computed point in space and the source [37]:

$$\text{NSS} = \frac{3\mu_0 m}{4\pi r^4} \tag{2.39}$$

From which it is also evident that it is a rotational invariant (since it dipends only on the distance r) and also that it does not depend on the direction of the magnetic moment $\mathbf{m}$, only on its magnitude.

2.4.1 Demonstration of Rotation Invariance

Let's define the gradient operator ∇ in any Cartesian coordinate system (x, y, z), given by

$$\nabla = \begin{bmatrix} \frac{\partial}{\partial x} \\ \frac{\partial}{\partial y} \\ \frac{\partial}{\partial z} \end{bmatrix}$$

as a column vector.
Let (x, y, z) be the Cartesian coordinates in the original frame, and (x', y', z') denote the coordinates in a rotated frame. The rotation is defined by a rotation matrix, which for simplicity, we assume to be a rotation around the z-axis by an angle θ:

$$\mathbf{R}_z(\theta) = \begin{pmatrix} \cos\theta & -\sin\theta & 0 \\ \sin\theta & \cos\theta & 0 \\ 0 & 0 & 1 \end{pmatrix}$$

The new coordinates (x', y', z') after the rotation are related to the original coordinates by:

$$\begin{bmatrix} x' \\ y' \\ z' \end{bmatrix} = \mathbf{R}_z(\theta) \begin{bmatrix} x \\ y \\ z \end{bmatrix}$$

Using the chain rule, we express the derivatives with respect to the rotated coordinates in terms of the original derivatives:

$$\frac{\partial}{\partial x'} = \cos(\theta)\frac{\partial}{\partial x} - \sin(\theta)\frac{\partial}{\partial y}$$

$$\frac{\partial}{\partial y'} = \sin(\theta)\frac{\partial}{\partial x} + \cos(\theta)\frac{\partial}{\partial y}$$

$$\frac{\partial}{\partial z'} = \frac{\partial}{\partial z}$$

Thus, the gradient operator in the rotated coordinate system can be expressed in matrix form as:

$$\nabla' = \mathbf{R}\nabla \tag{2.40}$$

Now, let $\mathbf{B}$ be a 3D vector field exspressed as a column vector as well:

$$\mathbf{B}(x, y, z) = \begin{bmatrix} B_x(x, y, z) \\ B_y(x, y, z) \\ B_z(x, y, z) \end{bmatrix}$$

The components of the vector field after the rotation are given by:

$$\mathbf{B}' = \mathbf{R}_z(\theta)\mathbf{B} \tag{2.41}$$

Then, we can rewrite the definition of the gradient tensor 1.1, in matrix form [1]:

$$\mathbf{G} = \nabla\mathbf{B}^T$$

Which becomes in the rotated coordinates (x', y', z'):

$$\mathbf{G}' = \nabla'\mathbf{B}'^T$$

Thus, substituting 2.40 and 2.41 into the expression for G', we obtain:

$$\mathbf{G}' = \mathbf{R} \nabla \, (\mathbf{R}\mathbf{B})^T$$

Using the linear algebra property of the transpose of the product of two matrices:

$$\mathbf{G}' = \mathbf{R} \nabla \, (\mathbf{B}^T \mathbf{R}^T)$$

Recognizing that $\nabla \, \mathbf{B}^T$ is the original gradient $\mathbf{G}$, we finally obtain the same result as [1]:

$$\mathbf{G}' = \mathbf{R} \, \mathbf{G} \, \mathbf{R}^T \tag{2.42}$$

Firstly, we focus on the eigenvalues of $\mathbf{G}$, namely λ_{min}, λ_{med}, and λ_{max}. To demonstrate rotational invariance, we recall the characteristic polynomial 2.35, which defines the eigenvalues of $\mathbf{G}$. Under a coordinate rotation, the tensor $\mathbf{G}$ transforms as shown in (2.42). Then, the characteristic equation for the rotated tensor is:

$$\det(\mathbf{G}' - \lambda \mathbf{I}) = \det\Big(\mathbf{R}\mathbf{G}\mathbf{R}^T - \lambda \mathbf{I}\Big)$$

Using Binet's Theorem and the property of orthogonal matrices $\det\left(\mathbf{R}\right) = \det\left(\mathbf{R}^T\right) = 1$:

$$\det\left(\mathbf{R}(\mathbf{G} - \lambda \mathbf{I})\mathbf{R}^T\right) = \det\left(\mathbf{G} - \lambda \mathbf{I}\right)$$

Consequently, the eigenvalues λ_{min}, λ_{med}, and λ_{max} of the tensor $\mathbf{G}$ remain unchanged, proving that they are rotationally invariant.
Secondly, we now demonstrate how I_2 and I_3 are rotational invariants with respect to a rotation of the coordinates systems. I_2 is defined as the sum of the principal minors of order 2 of $\mathbf{G}$. From linear algebra we know that the sum of principal minors is a linear combination of the eigenvalues of a matrix, which are in turn rotational invariants, as we just demonstrated, therefore I_2 is a rotational invariant as well.
Similarly, the determinant of $\mathbf{G}$, I_3, is also invariant under orthogonal transformations. This is agian due to the fact that the determinat of orthogonal matrices is 1 and thanks to Binet's Theorem:

$$\det\left(\mathbf{G}'\right) = \det\left(\mathbf{R}\mathbf{G}\mathbf{R}^T\right) = \det\left(\mathbf{R}\right) \det\left(\mathbf{G}\right) \det\left(\mathbf{R}^T\right) = \det\left(\mathbf{G}\right).$$

As I_2 and I_3 are constructed respectively from the sum of principal minors and the determinant of $\mathbf{G}$, both quantities remain invariant under any rotation of the coordinate system.

Chapter 3

Mathematical Model

3.1 Single Victim Case

Three Cartesian coordinate frames are defined as [33] and shown in 3.1:

(i) Frame i (inertial): denoted as $F_i = (O_i, x_i, y_i, z_i)$, is the inertial frame with origin O_i.

(ii) Frame r (receiver ARTVA): denoted as $F_r = (O_r, x_r, y_r, z_r)$, is the body right-hand frame associated with the receiver installed on the drone.

(iii) Frame t (transmitter ARTVA): denoted as $F_t = (O_t, x_t, y_t, z_t)$, is the body right-hand frame associated with the transmitter worn by the victim.

For the sake of simplicity, we assume that the body frame of the drone coincides with F_r. The position of O_r relative to O_t is indicated by the vector $\mathbf{p}_{tr} \in \mathbb{R}^3$, with $\mathbf{p}_{tr} = \mathbf{p}_r - \mathbf{p}_t$, while the positions of O_r and O_t relative to O_i are indicated, respectively, by the vectors $\mathbf{p}_r \in \mathbb{R}^3$ and $\mathbf{p}_t \in \mathbb{R}^3$. We use the apex i, r or t on the left of the vector to indicate in which frame the vector is expressed , e.g. ${}^t p$. If it is not specified, we assume the inertial frame.

Figure 3.1 Inertial frames in the single victim case

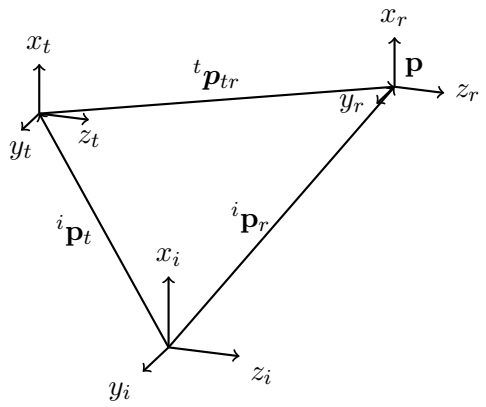

3.1.1 Magnitude of Magnetic Field Intensity H

We have found an expression of $\mathbf{H}$ in spherical coordinates, 2.27, whose magnitude is found as:

$$|\mathbf{H}| = \frac{Ib^2}{4\,r^3}\sqrt{4\cos^2\theta + \sin^2\theta} = \frac{Ib^2}{4\,r^3}\sqrt{3\cos^2\theta + 1} \tag{3.1}$$

Approximation

We use the same approximation in [33] in order to remove the non-linearity given by the square root term $\sqrt{3\cos^2\theta + 1}$. Therefore we approximate:

$$\frac{1}{\sqrt[3]{3\cos^2\theta + 1}} \approx \frac{1}{a^2}\cos^2\theta + \frac{1}{b^2}\sin^2\theta$$

of which the polar plot is shown in Figure 3.2 when a and b have values 1.291 and 1.028, respectively, which minimize the relative mean squared error = 0.123%.

Thus, the square root term becomes:

$$\sqrt{3\cos^2\theta + 1} \approx \frac{1}{\left(\frac{1}{a^2}\cos^2\theta + \frac{1}{b^2}\sin^2\theta\right)^{3/2}} \tag{3.2}$$

Using the approximation (3.2) in (3.1):

$$|\mathbf{H}| = \frac{Ib^2}{4\,r^3}\left(\frac{1}{a^2}\cos^2\theta + \frac{1}{b^2}\sin^2\theta\right)^{2/3} \tag{3.3}$$

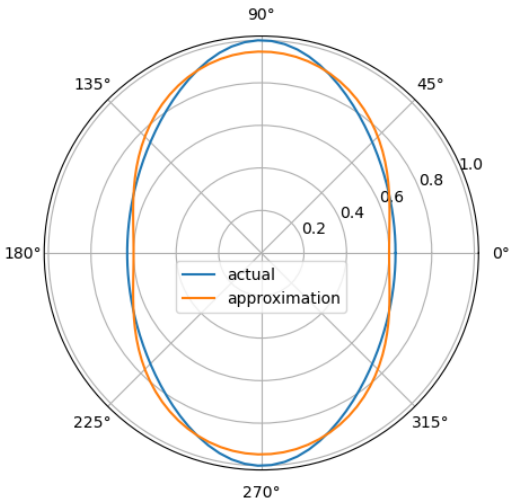

Figure 3.2 Polar plot of the actual function $\sqrt{3\cos^2\theta + 1}$ in blue and the approximated one $\frac{1}{a^2}\cos^2\theta + \frac{1}{b^2}\sin^2\theta$ in orange.

Now we can express the magnitude using the Cartesian coordinates relative to the frame of the transmitter ARTVA F_t. If we consider the point ${}^t\mathbf{p}_{tr}$

$${}^t\mathbf{p}_{tr} = \begin{pmatrix} x \\ y \\ z \end{pmatrix}$$

having these coordinates (x, y, z) in frame t, then remembering r from 1.8.1 and $\cos\theta$ from 1.8.2:

$$\begin{cases} r^2 = x^2 + y^2 + z^2 \\ \cos\theta = \frac{x}{r} \end{cases}$$

Substituting the expressions for r and $\cos\theta$ in 3.3:

$$|\mathbf{H}| = \frac{Ib^2}{4} \frac{1}{(x^2+y^2+z^2)^3} \left(\frac{1}{a^2} \frac{x^2}{x^2+y^2+z^2} + \frac{1}{b^2} \frac{y^2+z^2}{x^2+y^2+z^2} \right)^{2/3}$$

After simplifications and further calculations, we obtain:

$$|\mathbf{H}| = \frac{m}{4\pi} \left(\frac{(ab)^2}{b^2x^2 + a^2(y^2+z^2)} \right)^{3/2} \tag{3.4}$$

where we call $I\,\pi\,b^2$ the magnetic moment m, as seen in 2.31. Then, we can define η as [33]:

$$\eta = \left(\frac{m}{4\pi\,|\mathbf{H}|} \right)^{2/3} \cdot\ (ab)^2 =$$

by substituting 3.4:

$$= \left(\frac{m}{4\pi \frac{m}{4\pi} \left(\frac{(ab)^2}{b^2x^2+a^2(y^2+z^2)} \right)^{3/2}} \right)^{2/3} \cdot (ab)^2 =$$

$$= \left(\left(\frac{b^2x^2 + a^2(y^2+z^2)}{(ab)^2} \right)^{3/2} \right)^{2/3} \cdot (ab)^2$$

So:

$$\eta = b^2x^2 + a^2(y^2+z^2) \tag{3.5}$$

3.1.2 Finding the ARTVA position

In order to find the victim's position $\mathbf{p}_t$ with respect to the inertial frame F_i, we need to use homogeneous transformations [8]. Also from Figure 3.1, we can express the position of the receiver $\mathbf{p}_r$ in the inertial frame as the sum of the other two vectors:

$$^i\mathbf{p}_r = {}^i\mathbf{p}_t + {}^t\mathbf{p}_{tr}$$
$$^t\mathbf{p}_{tr} = \mathbf{R}_t^i\ {}^i\mathbf{p}_{tr}$$

where $\mathbf{R}_t^i$ is the rotation matrix that rotates axis i to t [26].

From which we can find $\mathbf{p}_t$ by multiplying by $\mathbf{R}_t^{iT}$ since $\mathbf{R}_t^i$ is orthogonal ($\mathbf{R}_t^{iT} = \mathbf{R}_t^{i-1}$):

$$^t\mathbf{p}_{tr} = \mathbf{R}_t^{iT}(\mathbf{p}_r - \mathbf{p}_t) \tag{3.6}$$

In addition, remembering how we defined the coordinates of $^t\mathbf{p}_{tr}$, then from linear algebra:

$$x = \mathbf{e}_x^T\ {}^t\mathbf{p}_{tr}$$
$$y = \mathbf{e}_y^T\ {}^t\mathbf{p}_{tr}$$
$$x = \mathbf{e}_z^T\ {}^t\mathbf{p}_{tr}$$

also,

$$x^2 = x \cdot x = \left(\mathbf{e}_x^T\, {}^t\mathbf{p}_{tr}\right)^T \cdot \left(\mathbf{e}_x^T\, {}^t\mathbf{p}_{tr}\right)$$

and the same is valid for the other two coordinates, we will omit the calculations for the other two from now on. We can then substitute the expression we found for ${}^t\mathbf{p}_{tr}$ 3.6 and apply linear algebra properties of the transpose:

$$(\mathbf{ABC})^T = \mathbf{C}^T\mathbf{B}^T\mathbf{A}^T$$

to calculate the transpose of $\mathbf{e}_x^T\mathbf{R}_t^{iT}(\mathbf{p}_r - \mathbf{p}_t)$:

$$(\mathbf{e}_x^T\mathbf{R}_t^{iT}(\mathbf{p}_r - \mathbf{p}_t))^T = (\mathbf{p}_r - \mathbf{p}_t)^T\mathbf{R}_t^i\mathbf{e}_x$$

The expression for x^2 then becomes:

$$x^2 = (\mathbf{p}_r - \mathbf{p}_t)^T\, \mathbf{R}_t^i\mathbf{e}_x\mathbf{e}_x^T\mathbf{R}_t^{iT}\, (\mathbf{p}_r - \mathbf{p}_t) \tag{3.7}$$

Furthermore:

$$\mathbf{e}_x\mathbf{e}_x^T = \begin{pmatrix}1\\0\\0\end{pmatrix}\begin{pmatrix}1 & 0 & 0\end{pmatrix} = \text{diag}(1,0,0)$$

and:

$$\mathbf{e}_y\mathbf{e}_y^T = \text{diag}(0,1,0)$$
$$\mathbf{e}_z\mathbf{e}_z^T = \text{diag}(0,0,1)$$

Lastly we substitute the result found in 3.7 in the expression of η 3.5:

$$\begin{aligned}\eta = {}& b^2\,(\mathbf{p}_r - \mathbf{p}_t)^T\, \mathbf{R}_t^i\mathbf{e}_x\mathbf{e}_x^T\mathbf{R}_t^{iT}\, (\mathbf{p}_r - \mathbf{p}_t) + \\ &+ a^2\,(\mathbf{p}_r - \mathbf{p}_t)^T\, \mathbf{R}_t^i\mathbf{e}_y\mathbf{e}_y^T\mathbf{R}_t^{iT}\, (\mathbf{p}_r - \mathbf{p}_t) + \\ &+ a^2\,(\mathbf{p}_r - \mathbf{p}_t)^T\, \mathbf{R}_t^i\mathbf{e}_z\mathbf{e}_z^T\mathbf{R}_t^{iT}\, (\mathbf{p}_r - \mathbf{p}_t) =\end{aligned}$$

collect common terms,

$$\begin{aligned}&= (\mathbf{p}_r - \mathbf{p}_t)^T\, \mathbf{R}_t^i \left(b^2\mathbf{e}_x\mathbf{e}_x^T + a^2\mathbf{e}_y\mathbf{e}_y^T + a^2\mathbf{e}_z\mathbf{e}_z^T\right) R_t^{iT}\, (\mathbf{p}_r - \mathbf{p}_t) = \\ &= (\mathbf{p}_r - \mathbf{p}_t)^T\, \mathbf{R}_t^i\, \text{diag}(b^2, a^2, a^2)\mathbf{R}_t^{iT}\, (\mathbf{p}_r - \mathbf{p}_t)\end{aligned} \tag{3.8}$$

We call the $\mathbf{R}_t^i\, \text{diag}(b^2, a^2, a^2)\mathbf{R}_t^{iT}$ matrix $\mathbf{M}$ and the diagonal matrix $\text{diag}(b^2, a^2, a^2)$ D.

Symmetry of $\mathbf{M}$

Definition
A matrix $\mathbf{M} \in \mathbb{R}^{n\times n}$ is symmetric if and only if $\mathbf{M} = \mathbf{M}^T$.
Proof
We compute $\mathbf{M}^T$:

$$\mathbf{M}^T = \left(\mathbf{R}_t^i\mathbf{D}\mathbf{R}_t^{iT}\right)^T = \left(\mathbf{R}_t^{iT}\right)^T\, \mathbf{D}^T\mathbf{R}_t^{iT} = \mathbf{R}_t^i\mathbf{D}^T\mathbf{R}_t^{iT}$$

Since $\mathbf{D}$ is a diagonal matrix, it is equal to its transpose $\mathbf{D}^T = \mathbf{D}$:

$$\mathbf{M}^T = \mathbf{R}_t^i D\mathbf{R}_t^{iT} = \mathbf{M}$$

Final expression for η

By applying the distributive property to 3.8 and since M is symmetric:

$$\eta = \mathbf{p}_r^T \mathbf{M} \mathbf{p}_r - \mathbf{p}_r^T \mathbf{M} \mathbf{p}_t - \mathbf{p}_t^T \mathbf{M} \mathbf{p}_r + \mathbf{p}_t^T \mathbf{M} \mathbf{p}_t \tag{3.9}$$

The vector $\hat{\mathbf{p}}_t$ gives an estimate of the true position $\mathbf{p}_t$:

$$\hat{\mathbf{p}}_t = \mathbf{M} \mathbf{p}_t$$

and since M is symmetric:

$$\hat{\mathbf{p}}_t^T = \mathbf{p}_t^T \mathbf{M}^T = \mathbf{p}_t^T \mathbf{M}$$

We substitute these expressions in 3.9 and use the definition of the scalar product:

$$\eta = \mathbf{p}_r^T \mathbf{M} \mathbf{p}_r - \mathbf{p}_r^T \hat{\mathbf{p}}_t - \hat{\mathbf{p}}_t^T \mathbf{p}_r + \mathbf{p}_t^T \mathbf{M} \mathbf{p}_r = \mathbf{p}_r^T \mathbf{M} \mathbf{p}_r - 2\mathbf{p}_r^T \hat{\mathbf{p}}_t + \mathbf{p}_t^T \mathbf{M} \mathbf{p}_t$$

If we define the coordinates of $\mathbf{p}_r$:

$$\mathbf{p}_r = \begin{pmatrix} x_r \\ y_r \\ z_r \end{pmatrix}$$

and

$$\mathbf{M} = \begin{pmatrix} m_{11} & m_{12} & m_{13} \\ m_{12} & m_{22} & m_{23} \\ m_{13} & m_{23} & m_{33} \end{pmatrix}$$

we can compute $\mathbf{p}_r^T \mathbf{M} \mathbf{p}_r$:

$$\mathbf{p}_r^T \mathbf{M} \mathbf{p}_r = m_{11}\, x_r^2 \;+\; 2\, m_{12}\, x_r\, y_r \;+\; 2\, m_{13}\, z_r\, x_r \;+\; m_{22}\, y_r^2 \;+\; 2\, m_{23}\, y_r\, z_r \;+\; m_{33}\, z_r^2$$

Then, we obtain a final expression for η as in [33]:

$$\begin{aligned} \eta = {} & m_{11}\, x_r^2 + 2\, m_{12}\, x_r\, y_r + 2\, m_{13}\, z_r\, x_r \\ & + m_{22}\, y_r^2 + 2\, m_{23}\, y_r\, z_r + m_{33}\, z_r^2 \\ & - 2\, x_r\, x_t - 2\, y_r\, y_t - 2\, z_r\, z_t \\ & + \mathbf{p}_t^T \mathbf{M} \mathbf{p}_t \end{aligned} \tag{3.10}$$

3.1.3 Finding the NSS

In the only one victim case, we can find the the NSS not only numerically but also analytically. Which means that since we have an expression of the magnetic field intensity $\mathbf{H}$ in Cartesian coordinates 2.28, we can compute the derivatives and therefore the gradient tensor $\mathbf{G}$ analytically as:

$$\mathbf{G} = \frac{1}{r^{5/2}} \begin{bmatrix} 3x(-2x^2+3y^2+3z^2) & 3y(-4x^2+y^2+z^2) & 3z(-4x^2+y^2+z^2) \\ 3y(-4x^2+y^2+z^2) & 3x(x^2-4y^2+z^2) & -15xyz \\ 3z(-4x^2+y^2+z^2) & -15xyz & 3x(x^2+y^2-4z^2) \end{bmatrix} \tag{3.11}$$

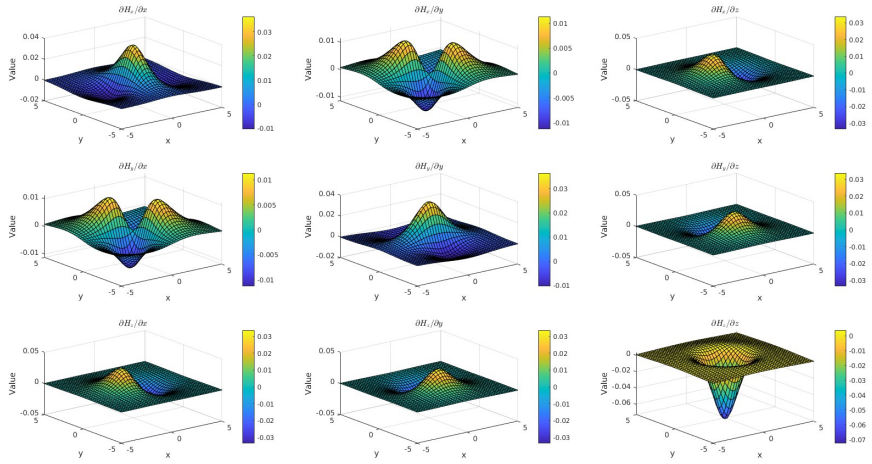

Figure 3.3 Plot of the gradients $\frac{\partial H_i}{\partial i}$ where $i = x, y, z$ which are the componets of the gradient tensor $\mathbf{G}$ when computed analytically as in 3.11, in the case of a single source located at the center $(0, 0)$ of the space when there are no rotations between the coordinates frames F_i, F_r, F_t.

where r is of course the distance, $r = \sqrt{x^2 + y^2 + z^2}$.

Note once again the symmetry and traceless property of the gradient tensor $\mathbf{G}$ is evident, when we compute it explicitly. Also note that for simplicity we computed the gradient using $\mathbf{H}$ and not $\mathbf{B}$, since they vary only by the constant permeability μ. We also omitted the constants I, b, since they don't depend on the coordinates (x, y, z) neither, and therefore do not influence the results.

In Figure 3.3, we show the gradients for a single source centered at the origin of the space, when the inertial frame F_i coincides with the trasmitter (source) frame F_t and also when there is no rotation between these frames and the receiver frame F_r of the drones. In this way, we have that the magnetic field intensity ${}^t\mathbf{H} = {}^i\mathbf{H}$ can be computed using the inertial coordinates, and also the NSS at any point in space coincides with the signal received by any drone located at that point. The gradients are calculated on a grid of equally spaced points in the range $[-5, 5]$, when we fix the z coordinates at 3 m, considering a reasonable flying height for the drones. We need to fix one coordinate in order to be able to plot a function of 3 variables, but also because we assume the drones flying always at a fixed height, as it will be explained more in depth lately.

After having found the gradient tensor $\mathbf{G}$, we numerically compute its eigenvalues and we find the NSS using the definition 2.38. In Figure 3.4, we plot the NSS distribution over the same grid, with the same z value fixed. These values will be the signals received by the drones at their location in space in the multiple victims case, which will be explained more in depth in the following paragraph.

Instead, let's consider the case when the source location is translated with respect to the inertial frame F_i and the transmitter frame F_t is rotated with respect to the inertial by a rotation $\mathbf{R}_t^i$, like in the previous section. Furthermore, we also consider the rotation $\mathbf{R}_r^t$ between the transmitter frame and the receiver frame F_r. Then, we compute the coordinates of any point in space with respect to the transmitter frame as in 3.6. Using these coordinates we find the magnetic intensity vector ${}^t\mathbf{H}$, expressed in the trasmitter frame and compute the

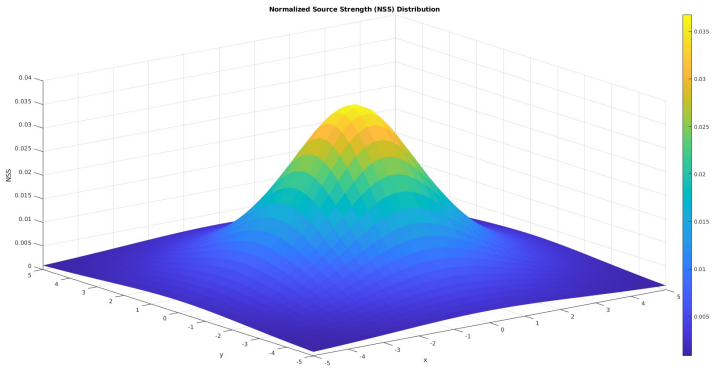

Figure 3.4 Plot of the NSS values computed at each point on the grid, which represent the signal received by the drones, in the case of a single source located at the center $(0, 0)$ of the space when there are no rotations between the coordinates frames F_i, F_r, F_t..

gradient tensor ${}^t\mathbf{G}$. Then, as we defined the $\mathbf{R}_t^i$ the matrix that rotates axis i to t, we find the gradient tensor ${}^i\mathbf{G}$ by inverting equation 2.42:

$$ {}^i\mathbf{G} = \mathbf{R}_t^{i\,T}\, {}^t\mathbf{G}\, \mathbf{R}_t^i \tag{3.12} $$

In Figure 3.5, we see how the gradients plots vary with respect to the gradients in Figure 3.3, since the rotations introduce naturally a modification in the elettromagnetic field. However, in Figure 3.6 it is also evident how the NSS distribution remains invariant under all the different rotations, and it is just affected by the translation in the sense that the peak now is located at the new location of the source.

However, for the multiple victims case we cannot compute the gradient tensor analytically and therefore we adopt a numerical approach. We simulate and simplify the way the authors of [37] use a cubic structure measurement array composed of eight tri-axial magnetometers in order to obtain the magnetic field information and therefore compute the gradient tensor $\mathbf{G}$. Let's consider a small perturbation δ in order to apply the central difference method approximation. We perturb the magnetic field intensity $\mathbf{H}$ by every direction

The gradient of a 3D vector field $\mathbf{f}(\mathbf{p})$, where $\mathbf{p} = (x, y, z)$, can be numerically approximated using the central difference method. Let δ be a small perturbation applied to each coordinate direction. The partial derivative of $\mathbf{f}$ with respect to a coordinate p_k is given by:

$$ \frac{\partial \mathbf{f}}{\partial p_k} \approx \frac{\mathbf{f}(\mathbf{p} + \delta \mathbf{e}_k) - \mathbf{f}(\mathbf{p} - \delta \mathbf{e}_k)}{2\delta}, $$

where $\mathbf{e}_k$ denotes the unit vector in the k-th direction. The gradient matrix, or Jacobian $\mathbf{J}$, is constructed by repeating this process for each coordinate direction:

This method, based on the Taylor series expansion, yields a second-order accurate estimate of the gradient by approximating the derivative as a difference of function values at perturbed points.

For a small perturbation δ, let $\boldsymbol{\delta}_k$ be a vector with δ in the k-th position. The perturbed points are:

$$ \mathbf{p}_k^+ = \mathbf{p} + \boldsymbol{\delta}_k, \quad \mathbf{p}_k^- = \mathbf{p} - \boldsymbol{\delta}_k. $$

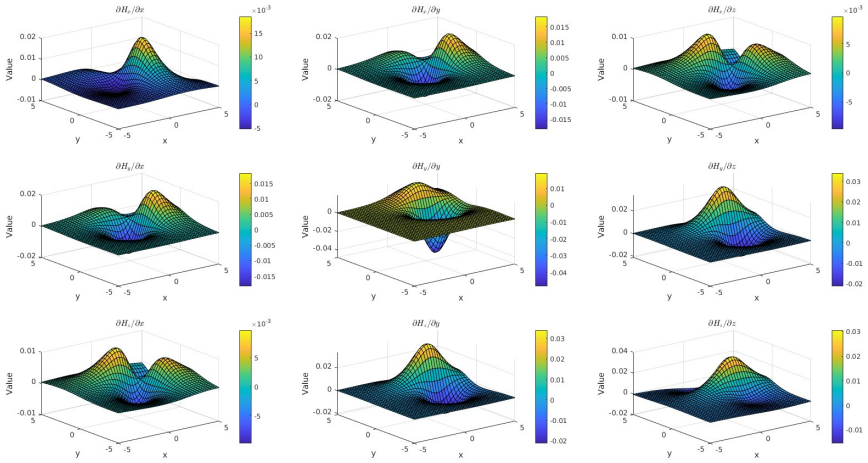

Figure 3.5 Plot of the gradients $\frac{\partial H_i}{\partial i}$ where $i = x, y, z$ when computed analytically after the position of the signle source is translated to $(2, 2)$ and an introduction of the different roations, expressed using $\mathbf{R}_r^t$ and $\mathbf{R}_t^i$.

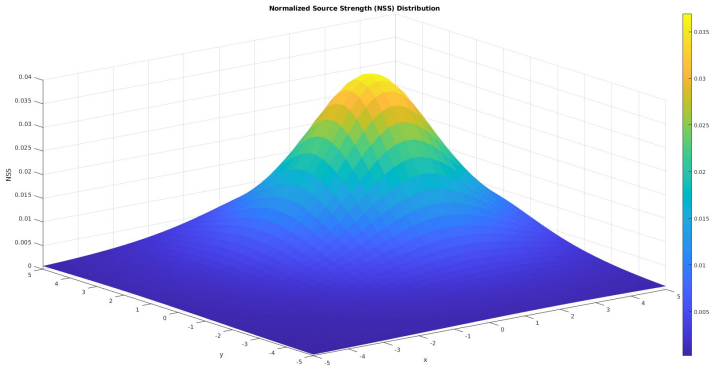

Figure 3.6 Plot of the NSS after the position of the signle source is translated to $(2, 2)$ and different roations are introduced, expressed using $\mathbf{R}_r^t$ and $\mathbf{R}_t^i$.

Figure 3.7 Only 2 victims case

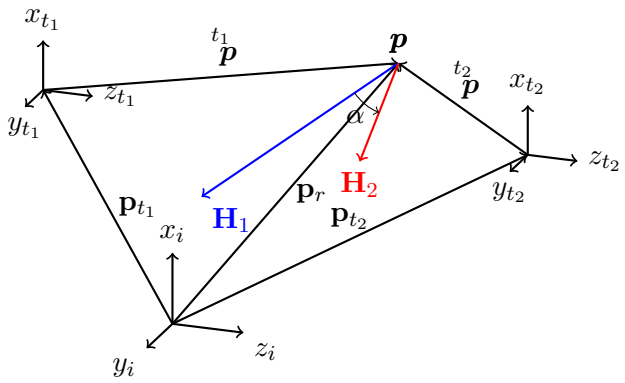

The k-th column of $\mathbf{J}$ is:

$$\mathbf{J}_{:,k} = \frac{\mathbf{f}(\mathbf{p}_k^+) - \mathbf{f}(\mathbf{p}_k^-)}{2\delta}.$$

General Formula:

$$\frac{\partial f_i}{\partial p_k} \approx \frac{f_i(\mathbf{p}_k^+) - f_i(\mathbf{p}_k^-)}{2\delta}.$$

3.2 Multiple Victim Case

In the multiple victim case an ARTVA transmitter is attached to every one of the n avalanche victims, therefore each receiver is affected by n generated electromagnetic fields. In Figure 3.7, the two victims case is represented, using the same frames as the single victim one. For brevity we will call R_1 and R_2 the relative orientations of frames t_1 and t_2 with respect to the reference frame i.

Now, if the receiver is positioned at point $\mathbf{p}$ in space, the summed effect of the electromagnetic fields can be expressed as the sum of the magnetic field intensity vector fields $\mathbf{H}_n$:

$$\mathbf{H}_{\text{tot}} = \mathbf{H}_1 + \mathbf{H}_2 + \cdots + \mathbf{H}_n$$

For the single magnetic field intensity vector of the i-th victim, remembering 2.27:

$$\mathbf{H}_i = \frac{Ib^2}{4\pi r^3} \left(\mathbf{e}_{r_i}\, 2\cos\theta + \mathbf{e}_{\theta_i}\, \sin\theta\right)$$

Furthermore, we use the same homogeneous transformations as 3.6:

$$\mathbf{p}_{t_1} + R_1\, \mathbf{p}^{t_1} = \mathbf{p}_r$$

$$\mathbf{p}_{t_2} + R_2\, \mathbf{p}^{t_2} = \mathbf{p}_r$$

which become again:

$$\mathbf{p}^{t_1} = R_1^T\, (\mathbf{p}_R - \mathbf{p}_{t_1})$$
$$\mathbf{p}^{t_2} = R_2^T\, (\mathbf{p}_R - \mathbf{p}_{t_2})$$

3.2.1 Total Magnitude

Suppose the case of only two victims, the results can be then generalized. If α is the angle between the two vectors $\mathbf{H}_1$ and $\mathbf{H}_2$ on the only plane which contains both vector fields, we have:

$$||\mathbf{H}_{\text{tot}}||^2 = ||\mathbf{H}_1||^2 + ||\mathbf{H}_2||^2 + 2\,||\mathbf{H}_1||\,||\mathbf{H}_2||\cos\alpha$$

Substituting the formula of the magnetic field magnitude after the approximation, with the Cartesian coordinates of reference frame F_t 3.4:

$$\begin{aligned}
||\mathbf{H}_{\text{tot}}||^2 &= \left(\frac{m}{4\pi}\right)^2 \left(\frac{(ab)^2}{b^2\,x_1^2 + a^2\,(y_1^2 + z_1^2)}\right)^3 + \left(\frac{m}{4\pi}\right)^2 \left(\frac{(ab)^2}{b^2\,x_2^2 + a^2\,(y_2^2 + z_2^2)}\right)^3 + \\
&+ 2\,\cos\alpha \left(\frac{m}{4\pi}\right)^2 \left(\frac{(ab)^2}{b^2\,x_1^2 + a^2\,(y_1^2 + z_1^2)}\right)^{3/2} \left(\frac{(ab)^2}{b^2\,x_2^2 + a^2\,(y_2^2 + z_2^2)}\right)^{3/2} = \\
&= \left(\frac{m\,(ab)^3}{4\pi}\right)^2 \left(\left(\frac{1}{b^2\,x_1^2 + a^2\,(y_1^2 + z_1^2)}\right)^3 + \left(\frac{1}{b^2\,x_2^2 + a^2\,(y_2^2 + z_2^2)}\right)^3 + \right. \\
&\left. + 2\,\cos\alpha \left(\frac{1}{(b^2\,x_1^2 + a^2\,(y_1^2 + z_1^2))(b^2\,x_2^2 + a^2\,(y_2^2 + z_2^2))}\right)^{3/2}\right)
\end{aligned}$$

Note that a and b, have the same values for all the fields since they have been chosen in order to optimize the magnitude on any magnetic field intensity. Also we suppose that the radius b and the current I are the same for all the devices (so same magnetic moment m).

Bringing the common terms to the left side and inverting all the fractions:

$$\begin{aligned}
\left(\frac{m\,(ab)^3}{4\pi\,||\mathbf{H}_{\text{tot}}||}\right)^2 &= \left(b^2\,x_1^2 + a^2\,(y_1^2 + z_1^2)\right)^3 + \left(b^2\,x_2^2 + a^2\,(y_2^2 + z_2^2)\right)^3 + \\
&+ 2\,\cos\alpha \left((b^2\,x_1^2 + a^2\,(y_1^2 + z_1^2))(b^2\,x_2^2 + a^2\,(y_2^2 + z_2^2))\right)^{3/2}
\end{aligned}$$

SPIEGARE PERchE QUESTO È UNFEASIBLE

3.2.2 Finding the NSS

Chapter 4

Literature Review

[27] This article proposes a new method to simultaneously estimate the locations and magnetic moments of multiple magnetic dipole sources without the prior knowledge of the number of dipoles in the 3-D detection region. By initializing a large number of dipole sources evenly spaced in the detection region as potential candidates for the true dipoles, we introduce an indicator parameter for each dipole candidate such that its Sigmoid function is the probability that the candidate converges to a true dipole. A joint optimization is then formulated to minimize the mean square of the regularized error between the measured magnetic gradients and the calculated gradients from the estimated dipoles. The proposed nonlinear optimization is solved by the Levenberg–Marquardt algorithm, yielding the indicators and their corresponding dipole locations and magnetic moments.

[25] Multi-magnetic source resolution in spacecraft has been a difficult problem in the field of magnetic surveys. Detection technology of magnetic gradient tensor is available to solve this issue due to its high resolution and precision. A spacecraft magnetic source model is established, and a multi-magnetic source model fitting method for spacecraft is presented. The principal invariants of the magnetic field gradient tensor are introduced to determine the number and horizontal location of the sources, while Euler equations are used to compute the source depth, achieving a resolution of up to 0.012m, which meets engineering requirements.

[4] Nothing much is a real application.

[23] Questo è il paper utile dove ci sono tutti i plot.

[34] This article presents a new method for detecting and localizing multiple dipole-like magnetic sources using magnetic gradient tensor data. The tilt angle (ratio of vertical to horizontal magnetic field components) is used to determine the number of sources, while the rotational-invariant normalized source strength (NSS) is used to estimate the horizontal coordinates. The Differential Evolution (DE) algorithm estimates the locations and moments of the sources.

[28] This paper presents a simple formula for the localization of a magnetic dipole. First, the position vector is derived from the analytical expressions of the magnetic field vector and the magnetic gradient tensor. The proposed algorithm provides the true position of the

dipole regardless of the singularity of the magnetic gradient tensor matrix.

[38] This paper proposes a new edge detection method using magnetic gradient tensor components for magnetic exploration, which is free from geomagnetic interference and provides abundant information. The method is compared with others, such as THDz, AS, tilt angle, and theta map, under various conditions. The experimental results show that the proposed method is more precise and delivers high-quality edge detection with strong anti-interference capabilities.

[35] This paper proposes a two-point magnetic gradient tensor localization model to overcome errors caused by geomagnetic fields. The model uses the spatial relation between the magnetic target and observation points derived from tensor invariants. A new method is presented for accurately locating magnetic targets, achieving nearly error-free results in the absence of noise.

[12] This paper introduces new methods for inverting magnetic gradient tensor data to obtain source parameters for various models, such as dipoles and thin sheets. Eigenvalues and eigenvectors of the tensor are used in combination with normalized source strength (NSS) to uniquely determine source locations. NSS analysis is extended to vertical pipes by calculating eigenvalues of the vertical derivative of the tensor.

[37] This article introduces a novel magnetic dipole localization method based on normalized source strength (NSS) to overcome asphericity errors in magnetic anomaly detection (MAD). A closed-form localization formula is derived, and an optimization method is proposed to improve noise immunity. Simulation and field experiments demonstrate high localization accuracy, real-time performance, and robustness against noise and misalignment errors.

[10] For a number of widely used models, normalized source strength (NSS) can be derived from eigenvalues of the magnetic gradient tensor. NSS is proportional to a constant normalized by the distance between observation and integration points. It is independent of magnetization direction and satisfies Euler's homogeneity equation, allowing for Euler deconvolution of the NSS to estimate source location. The method was applied to aeromagnetic data from the Tuckers Igneous Complex, Queensland, Australia, improving the interpretation of magnetic anomalies with strong remanent magnetization.

[5] Closed loop formula to find z.

[11] Recent technological advances suggest that we are on the threshold of a new era in applied magnetic surveys, where acquisition of magnetic gradient tensor data will become routine. In the meantime, modern ultrahigh resolution conventional magnetic data can be used, with certain important caveats, to calculate gradient tensor elements from total magnetic intensity (TMI) or TMI gradient surveys. Until the present, not a great deal of attention has been paid to processing and interpretation of gradient tensor data. New methods for inverting gradient tensor surveys to obtain source parameters have been developed for a number of elementary, but useful, models. These include point pole, line of poles, point dipole (sphere), line of dipoles (horizontal cylinder), thin and thick dipping sheets, sloping

step, and contact models. A key simplification is the use of eigenvalues and associated eigenvectors of the tensor. The scaled source strength, calculated from the eigenvalues, is a particularly useful rotational invariant that peaks directly over compact sources, 2D sources, and contacts, independent of magnetization direction. New algorithms for uniquely determining the location and magnetic moment of a dipole source from a few irregularly located measurements or single profiles have been developed. Besides geological applications, these algorithms are readily applicable to the detection, location, and classification (DLC) of magnetic objects, such as naval mines, UXO, shipwrecks, archaeological artifacts, and buried drums. As an example, some of these new methods are applied to analysis of the magnetic signature of the Mount Leyshon gold-mineralized system, Queensland.

[19] In this paper, a modified particle swarm optimization (PSO) algorithm is developed for solving multimodal function optimization problems. The difference between the proposed method and the general PSO is to split up the original single population into several subpopulations according to the order of particles. The best particle within each subpopulation is recorded and then applied into the velocity updating formula to replace the original global best particle in the whole population. To update all particles in each subpopulation, the modified velocity formula is utilized. Based on the idea of multiple subpopulations, for the multimodal function optimization, several optima including the global and local solutions may be found by these best particles separately. To show the efficiency of the proposed method, two kinds of function optimizations are provided, including a single modal function optimization and a complex multimodal function optimization. Simulation results will demonstrate the convergence behavior of particles by the number of iterations, and the global and local system solutions are solved by these best particles of subpopulations.

Chapter 5

Implementation

5.1 Introduction

Simulations have been done in MATLAB.

5.2 Particle Swarm Optimization

The PSO[1] algorithm was first introduced in 1995 [3], and it has since proven to be a powerful tool for solving various optimization problems. In the standard PSO algorithm, a population of particles is randomly initialized to represent potential candidate solutions for the optimization problem. Each particle relies on two important pieces of information: its individual best, referred to as *pbest*, and the global best across the entire population, referred to as *gbest*. These two values guide the search direction of all particles over the search space. The evaluation of the *pbest* for each particle and the *gbest* for the entire population is determined by the function that needs to be optimized.

In our implementation, each particle corresponds to an individual drone within the swarm, and the velocity and position of each drone are updated in accordance with the aforementioned standard PSO algorithm. Let $\mathbf{p}_i \in \mathbb{R}^2$ for $i = 1, 2, \ldots, n$ represent the position vectors of the drones in the 2D plane, where n is the total number of drones. The motion of each particle is governed by two fundamental equations: the velocity update equation (Eq. 5.1) and the position update equation (Eq. 5.2).

$$\mathbf{v}_i(t+1) = \omega\, \mathbf{v}_i(t) + c_1 r_1 \left(\mathbf{pbest}_i(t) - \mathbf{p}_i(t)\right) + c_2 r_2 \left(\mathbf{gbest}(t) - \mathbf{p}_i(t)\right) \tag{5.1}$$

$$\mathbf{p}_i(t+1) = \mathbf{p}_i(t) + \mathbf{v}_i(t+1) \tag{5.2}$$

where $\mathbf{p}_i$, $\mathbf{pbest}_i$, and $\mathbf{gbest}$ represent the position vector of the i-th particle, the i-th particle's individual best position vector, and the global best position vector, ω is the inertia weight, c_1 and c_2 are positive constants, and r_1 and r_2 are random variables uniformly distributed over the interval $[0, 1]$.

In the standard PSO algorithm, there is only one global best particle, which means that only one optimal solution can be found. This limitation poses a challenge when dealing with our problem, where we are looking for multiple sources, and therefore, multiple local and global optima exist. To address this challenge, we employ the same strategy of a modified

[1] PSO stands for Particle Swarm Optimization.

version of the PSO algorithm [19]. In this modification, the swarm is divided into M subpopulations, each tasked with exploring different regions of the search space. Following this idea, the *gbest* is referred to as the best particle of each subpopulation, not as the global best particle in the whole population. This means that these M best particles are separately able to catch different optima, at most M optima.

The function `sort_drones_in_groups` returns the number of groups and sorts the particles in different groups based on the following logic (see Algorithm 1):

Algorithm 1 `sort_drones_in_groups` (MATLAB function)

Inputs:
n_drones: Number of drones available for assignment
$n\_sources$: Number of sources to which drones need to be assigned
Outputs:
$group\_indices$: A vector of size n_drones indicating the assigned group
n_groups: The obtained number of groups
if $n\_particles > n\_sources$ **then**
    Assign at least one particle to each group, following mathematical order
    Randomly assign remaining particles to existing groups
else if $n\_particles = n\_sources$ **then**
    Assign each particle to a unique group
else
    Orderly assign particles up to n_drones
end if
Set the number of groups: $n\_groups = max(group\_indices)$

Note that the function `sort_drones_in_groups` ensures the creation of sufficient groups for the localization of multiple sources only when the number of drones is equal to or greater than the number of sources.

5.3 Exploration phase

Unlike the modified PSO algorithm, in our implementation, the drones are not randomly initialized. At the start of the simulation, all drones are located at the origin of the search space. An Exploration Phase begins where the PSO algorithm is not yet employed. During this phase, the drones move according to predefined trajectories at maximum speed $v_{\max}$. The trajectories are determined based on the number of drones and follow a radial pattern, as shown in Figure 5.1. The drones follow these trajectories until they have covered a distance $travel\_distance$ equivalent to half the boundary of the search space. The goal each drone needs to reach is computed using the following Algorithm 2:

Algorithm 2 `exploration_goals` (MATLAB function)

Input: n_drones, x_max
Output: $goals$
Initialize an empty array $goals$
Set $angle\_step = 360/n\_drones$
Set $travel\_distance = x\_max/2$
for each drone $i = 1, 2, \ldots, n\_drones$ **do**
    Get angle for the current drone: $drone\_angle = i \cdot angle\_step$
    Calculate slope: $m = \tan(\texttt{deg2rad}(drone\_angle))$
    if $drone\_angle > 315$ **or** $drone\_angle \leq 45$ **then**
        $goal = [travel\_distance, m \cdot travel\_distance]$ ▷ 1st quadrants
    else if $drone\_angle > 45$ **and** $drone\_angle \leq 135$ **then**
        $goal = [travel\_distance/m, travel\_distance]$ ▷ 2nd quadrant
    else if $drone\_angle > 135$ **and** $drone\_angle \leq 225$ **then**
        $goal = [-travel\_distance, m \cdot -travel\_distance]$ ▷ 3rd quadrant
    else if $drone\_angle > 225$ **and** $drone\_angle \leq 315$ **then**
        $goal = [-travel\_distance/m, -travel\_distance]$ ▷ 4th quadrant
    end if
    Store the goal for drone i in $goals[i]$
end for
Return $goals$

where $angle\_step$ is the angular increment to uniformly divide the space, $drone\_angle$ represents the angle assigned to each drone, determining its trajectory, while m is the slope of the trajectory calculated from the drone's angle.

5.4 Exploitation Phase

5.4.1 Velocity Update

At each time step, the velocity update of the standard PSO algorithm is modified in order to favor the complete exploration of the search space and to avoid premature convergence to local maxima, where a source is not present. A uniform random noise is added to the velocity of each particle to achieve a *persistence of excitation*, allowing every drone to explore new and different directions, as described in the following formula:

$$\mathbf{v}_i = \mathbf{v}_i + \beta \cdot \mathbf{r} \cdot ||\mathbf{v}_i||$$

where:

- β is an hyperparameter chosen in the [0,1] range.
- $\mathbf{r} \sim \mathcal{U}(-1, 1)$ represents a random vector where each component is uniformly distributed between -1 and 1.
- $||\mathbf{v}_i||$ is the magnitude of the velocity vector of particle i.

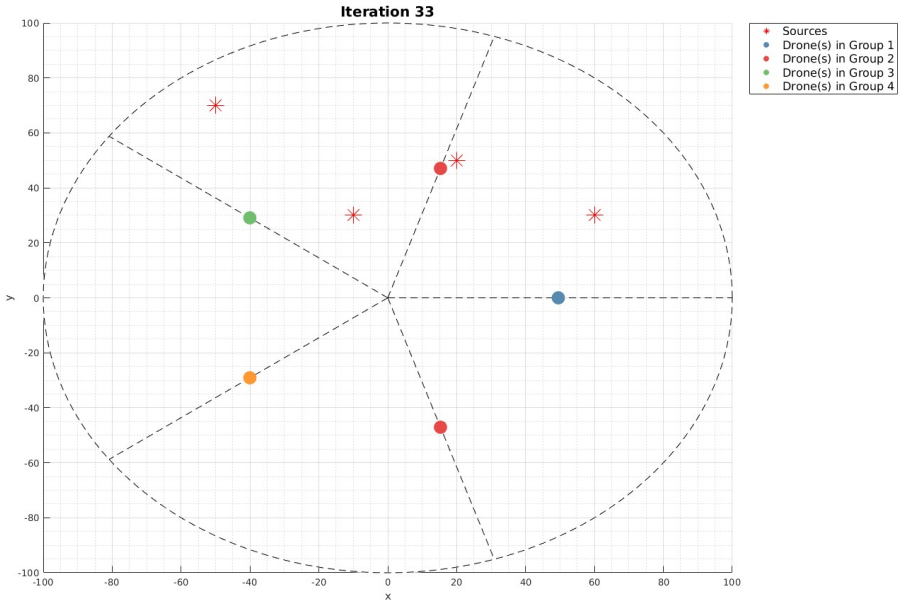

Figure 5.1 Radial exploration pattern for 5 drones at the end of the Exploration Phase.

Furthermore, not only because of the physical velocity limitations of the drones, but also to ensure smoother updates and prevent instability due to excessive velocity, we clamp the velocity of each drone to a maximum value $v_{\max}$:

$$\mathbf{v}_i = \begin{cases} v_{\max} \cdot \frac{\mathbf{v}_i}{\|\mathbf{v}_i\|}, & \text{if } \|\mathbf{v}_i\| \geq v_{\max} \\ \mathbf{v}_i, & \text{otherwise} \end{cases}$$

5.4.2 Exclusion Zone Mechanism

An additional modification to the standard PSO algorithm is the introduction of an exclusion zone mechanism. This mechanism prevents multiple drones from focusing on the same source. It involves defining regions that other particles should avoid, promoting better exploration and reducing redundancy in source detection. The exclusion zone mechanism involves several key parts:

- **Detection**: A drone sets its exclusion zone when it identifies a source with a signal strength (NSS) exceeding a predefined threshold.
- **Sharing**: The drone shares the position of its exclusion zone with neighboring drones.
- **Checking**: Each drone continuously checks its position against all shared exclusion zones.
- **Avoidance**: If a drone finds itself within a shared exclusion zone, it moves away from the zone following a calculated escape vector.

Detection

Each drone establishes an exclusion zone when it detects a source, meaning it has computed an NSS higher than a certain threshold. The exclusion zone is defined as a circular area centered around the position of the drone where the source was detected. The radius of this zone is a fixed parameter, chosen experimentally, which determines the *resolution* of the algorithm.

Sharing

Our algorithm favors a decentralized approach, which is useful in scenarios where communication between drones is not always possible or easy. A drone can communicate with another when they are less than 5 meters apart (r_{comm}). When a drone identifies a source and sets its exclusion zone, it shares the estimated position of the source with the drones within the communication range. Each drone maintains a list of exclusion zones that it has received from others. This sharing process helps the swarm avoid redundant exploration around already identified sources.

Avoidance

When a drone detects that it is within the radius of a shared exclusion zone, it is programmed to move away from it. The drone computes a new goal position where it needs to go, far from the exclusion zone . After it reaches the goal, the PSO algorithm resumes, searching for a new source in a different area of the space.

The goal position is calculated using the vector joining the exclusion zone center $\mathbf{c}$ and the current position of the drone $\mathbf{p}_{\text{in\_zone}}$, when the drone finds itself in an exclusion zone. The formula is given by:

$$\mathbf{d} = \mathbf{c} - \mathbf{p}_{\text{in\_zone}}$$

$$\mathbf{p}_{\text{goal}} = \mathbf{p}_{\text{in\_zone}} + \alpha \frac{\mathbf{d}}{\|\mathbf{d}\|}$$

where:

- $\mathbf{d}$: Direction vector from the exclusion zone center to the drone's position.
- α: Step size parameter, determining the distance the drone should travel away from the exclusion zone.
- $\mathbf{p}_{\text{goal}}$: Updated goal position of the drone.
- $\|\mathbf{d}\|$: Norm (magnitude) of the direction vector $\mathbf{d}$, used to normalize the direction.

This calculation ensures that the drone moves directly away from the exclusion zone and covers a distance proportional to α.

The exclusion zone mechanism allows the swarm to adaptively adjust its search strategy based on the locations of previously detected sources, leading to faster convergence and improved accuracy in multi-source localization. Finally, we can present the complete modified PSO algorithm in Algorithm 3: Note that the inertia of a drone that has found a source

Algorithm 3 Particle Swarm Optimization for Multi-Source Localization

Initialize drones' positions to the center of the search space.
Initialize group best positions G_{best} and values NSS_{best}.
Assign each drone to a group using function 1.
Exploration Phase:
Compute exploration goals using function 2.
for each drone i **do**
    Do: reach goal.
end for
Exploitation Phase:
for each iteration $t = 1$ to n_{iters} **do**
    for each drone i **do**
        Update velocity using standard PSO formula as in Eq.(5.1).
        Apply persistence of excitation as in Eq. (5.4.1).
        Limit velocity to v_{max} as in Eq. (5.4.1).
        Update position as in Eq. (5.2).
        Apply boundary conditions to keep $\mathbf{p}_i(t+1)$ within search bounds.
        for each other drone $j \neq i$ **do**
            if $\|\mathbf{p}_i(t+1) - \mathbf{p}_j(t+1)\| \leq r_{\text{comm}}$ **then**
                if NSS_i or $\text{NSS}_j >$ threshold **then**
                    Share exclusion zones between drones i and j.
                end if
            end if
        end for
        Check if drone i is within an exclusion zone.
        if drone i is in an exclusion zone **then**
            if drone i is not alone in its group **then**
                Reassign drone i to a new group.
                Initialize G_{best} and NSS_{best} of the new group.
            end if
            Move away from exclusion zone as in Eq. (5.4.2).
            Reset personal best $\mathbf{p}_{\text{best},i}$.
            Set drone i inertia $\omega = 0$.
        else
            Evaluate NSS at $\mathbf{p}_i(t+1)$.
            if current NSS $>$ personal best NSS **then**
                Update personal best $\mathbf{p}_{\text{best},i}$.
            end if
            if current NSS $>$ group best NSS **then**
                Update group best G_{best}.
            end if
        end if
    end for
end for
Return G_{best}.

is set to zero ($\omega = 0$), increasing convergence speed. Throughout the process, each drone updates its personal and group best positions based on newly evaluated NSS values, like in the standard PSO algorithm. The final output is the set of best estimates G_{best}, composed of the best estimated position of a source by each group.

Bibliography

[1] L. Pedersen and T. Rasmussen, "The gradient tensor of potential field anomalies: Some implications on data collection and data processing of maps," *Geophysics*, vol. 55, pp. 1558–1566, Dec. 1990. DOI: 10.1190/1.1442807.

[2] M. Falk, H. Brugger, and L. Adler-Kastner, "Avalanche survival chances," *Nature*, vol. 368, no. 6466, pp. 21–21, 1994.

[3] J. Kennedy and R. Eberhart, "Particle swarm optimization," in *Proceedings of ICNN'95 - International Conference on Neural Networks*, vol. 4, 1995, 1942–1948 vol.4. DOI: 10.1109/ICNN.1995.488968.

[4] P. Schmidt, D. Clark, K. Leslie, M. Bick, D. Tilbrook, and C. Foley, "Getmag - a squid magnetic tensor gradiometer for mineral and oil exploration," *Exploration Geophysics - EXPLOR GEOPHYS*, vol. 35, Dec. 2004. DOI: 10.1071/EG04297.

[5] T. Nara, S. Suzuki, and S. Ando, "A closed-form formula for magnetic dipole localization by measurement of its magnetic field and spatial gradients," *IEEE Transactions on Magnetics*, vol. 42, no. 10, pp. 3291–3293, 2006. DOI: 10.1109/TMAG.2006.879151.

[6] P. Pinies and J. Tardos, "Fast localization of avalanche victims using sum of gaussians," in *Proceedings 2006 IEEE International Conference on Robotics and Automation, 2006. ICRA 2006.*, 2006, pp. 3989–3994. DOI: 10.1109/ROBOT.2006.1642314.

[7] P. Pinies, J. D. Tardos, and J. Neira, "Localization of avalanche victims using robocentric slam," in *2006 IEEE/RSJ International Conference on Intelligent Robots and Systems*, 2006, pp. 3074–3079. DOI: 10.1109/IROS.2006.282247.

[8] B. Siciliano, L. Sciavicco, L. Villani, and G. Oriolo, *Robotics: Modelling, Planning and Control* (Advanced Textbooks in Control and Signal Processing). Springer London, 2010, ISBN: 9781846286414. [Online]. Available: https://books.google.it/books?id=jPCAFmE-logC.

[9] S. Waharte and N. Trigoni, "Supporting search and rescue operations with uavs," in *2010 International Conference on Emerging Security Technologies*, 2010, pp. 142–147. DOI: 10.1109/EST.2010.31.

[10] M. Beiki, D. A. Clark, J. R. Austin, and C. A. Foss, "Estimating source location using normalized magnetic source strength calculated from magnetic gradient tensor data," *Geophysics*, vol. 77, no. 6, J23–J37, 2012, ISSN: 0016-8033. DOI: 10.1190/geo2011-0437.1. [Online]. Available: https://doi.org/10.1190/geo2011-0437.1.

[11] D. Clark, "New methods for interpretation of magnetic gradient tensor data," *ASEG Extended Abstracts*, vol. 2012, Dec. 2012. DOI: 10.1071/ASEG2012ab081.

[12] D. Clark, "New methods for interpretation of magnetic vector and gradient tensor data i: Eigenvector analysis and the normalised source strength," *Exploration Geophysics*, vol. 43, pp. 267–282, Sep. 2012. DOI: 10.1071/EG12020.

[13] L. Marconi *et al.*, "The sherpa project: Smart collaboration between humans and ground-aerial robots for improving rescuing activities in alpine environments," in *2012 IEEE International Symposium on Safety, Security, and Rescue Robotics (SSRR)*, 2012, pp. 1–4. DOI: 10.1109/SSRR.2012.6523905.

[14] J. Marsden and A. Tromba, *Vector Calculus*. Macmillan Learning, 2012, ISBN: 9781429224048. [Online]. Available: https://books.google.it/books?id=pVbIygAACAAJ.

[15] T. Tomic *et al.*, "Toward a fully autonomous uav: Research platform for indoor and outdoor urban search and rescue," *IEEE Robotics & Automation Magazine*, vol. 19, no. 3, pp. 46–56, 2012. DOI: 10.1109/MRA.2012.2206473.

[16] D. Cheng, *Field and Wave Electromagnetics* (Addison-Wesley series in electrical engineering). Pearson Education Limited, 2014, ISBN: 9781292026565.

[17] D. Griffiths, *Introduction to Electrodynamics*. Pearson Education, 2014, ISBN: 9780321972101. [Online]. Available: https://books.google.it/books?id=J9ygBwAAQBAJ.

[18] G. Bevacqua, J. Cacace, A. Finzi, and V. Lippiello, "Mixed-initiative planning and execution for multiple drones in search and rescue missions," *Proceedings of the International Conference on Automated Planning and Scheduling*, vol. 25, no. 1, pp. 315–323, Apr. 2015. DOI: 10.1609/icaps.v25i1.13700. [Online]. Available: https://ojs.aaai.org/index.php/ICAPS/article/view/13700.

[19] W.-D. Chang, "A modified particle swarm optimization with multiple subpopulations for multimodal function optimization problems," *Applied Soft Computing*, vol. 33, pp. 170–182, 2015, ISSN: 1568-4946. DOI: https://doi.org/10.1016/j.asoc.2015.04.002. [Online]. Available: https://www.sciencedirect.com/science/article/pii/S1568494615002161.

[20] V. Ferrara, "Technical survey about available technologies for detecting buried people under rubble or avalanches," *WIT Transactions on the Built Environment*, vol. 150, pp. 91–101, 2015. [Online]. Available: https://api.semanticscholar.org/CorpusID:110028936.

[21] J. Cacace, A. Finzi, V. Lippiello, M. Furci, N. Mimmo, and L. Marconi, "A control architecture for multiple drones operated via multimodal interaction in search & rescue mission," in *2016 IEEE International Symposium on Safety, Security, and Rescue Robotics (SSRR)*, 2016, pp. 233–239. DOI: 10.1109/SSRR.2016.7784304.

[22] J. Cacace, A. Finzi, and V. Lippiello, "Implicit robot selection for human multi-robot interaction in search and rescue missions," in *2016 25th IEEE International Symposium on Robot and Human Interactive Communication (RO-MAN)*, 2016, pp. 803–808. DOI: 10.1109/ROMAN.2016.7745211.

[23] Y. Gang, Z. Yingtang, F. Hongbo, L. Zhining, and R. Guoquan, "Detection, localization and classification of multiple dipole-like magnetic sources using magnetic gradient tensor data," *Journal of Applied Geophysics*, vol. 128, pp. 131–139, 2016, ISSN: 0926-9851. DOI: https://doi.org/10.1016/j.jappgeo.2016.03.022. [Online]. Available: https://www.sciencedirect.com/science/article/pii/S0926985116300714.

[24] C. Sampedro, A. Rodriguez-Ramos, H. Bavle, A. Carrio, P. de la Puente, and P. Campoy, "A fully-autonomous aerial robot for search and rescue applications in indoor environments using learning-based techniques," *Journal of Intelligent & Robotic Systems*, vol. 95, pp. 601–627, 2018. [Online]. Available: https://api.semanticscholar.org/CorpusID:115873208.

[25] C. Xu, Z. Yi, L. Meng, K. Huang, and J. Dai, "Detection technology of multi-magnetic source in spacecraft based on magnetic field gradient tensor," *IOP Conference Series: Earth and Environmental Science*, vol. 237, p. 032 021, Mar. 2019. DOI: 10.1088/1755-1315/237/3/032021.

[26] J. Cacace, N. Mimmo, and L. Marconi, "A ros gazebo plugin to simulate arva sensors," in *2020 IEEE International Conference on Robotics and Automation (ICRA)*, 2020, pp. 7233–7239. DOI: 10.1109/ICRA40945.2020.9196914.

[27] S. Chang, Y. Lin, Y. R. Zheng, and X. Fu, "Simultaneous detection of multiple magnetic dipole sources," *IEEE Transactions on Magnetics*, vol. 56, no. 9, pp. 1–11, 2020. DOI: 10.1109/TMAG.2020.3011630.

[28] G. Yin, L. Zhang, H. Jiang, Z. Wei, and Y. Xie, "A closed-form formula for magnetic dipole localization by measurement of its magnetic field vector and magnetic gradient tensor," *Journal of Magnetism and Magnetic Materials*, vol. 499, p. 166 274, 2020, ISSN: 0304-8853. DOI: https://doi.org/10.1016/j.jmmm.2019.166274. [Online]. Available: https://www.sciencedirect.com/science/article/pii/S0304885319324448.

[29] I. A. Azzollini, N. Mimmo, L. Gentilini, and L. Marconi, "Uav-based search and rescue in avalanches using ARVA: an extremum seeking approach," *CoRR*, vol. abs/2106.14514, 2021. arXiv: 2106.14514. [Online]. Available: https://arxiv.org/abs/2106.14514.

[30] D. Eidenbenz *et al.*, "Survival probability in avalanche victims with long burial (≥60 min): A retrospective study," *Resuscitation*, vol. 166, pp. 93–100, 2021, ISSN: 0300-9572. DOI: 10.1016/j.resuscitation.2021.05.030. [Online]. Available: https://www.sciencedirect.com/science/article/pii/S0300957221002148.

[31] *ETSI EN 300 718-1 European Standard*, v2.2.1, Available at https://www.etsi.org/deliver/etsi_en/300700_300799/30071801/02.02.01_60/en_30071801v020201p.pdf, ETSI, Jun. 2021.

[32] N. Mimmo, P. Bernard, and L. Marconi, "Avalanche victim search via robust observers," *IEEE Transactions on Control Systems Technology*, vol. 29, no. 4, pp. 1450–1461, 2021. DOI: 10.1109/TCST.2020.3016665.

[33] C. Tabasso, N. Mimmo, V. Cichella, and L. Marconi, "Optimal motion planning for localization of avalanche victims by multiple uavs," *IEEE Control Systems Letters*, vol. 5, no. 6, pp. 2054–2059, 2021. DOI: 10.1109/LCSYS.2021.3049314.

[34] X. Ding, Y. Li, M. Luo, J. Chen, Z. Li, and H. Liu, "Estimating locations and moments of multiple dipole-like magnetic sources from magnetic gradient tensor data using differential evolution," *IEEE Transactions on Geoscience and Remote Sensing*, vol. 60, pp. 1–13, 2022. DOI: 10.1109/TGRS.2021.3094057.

[35] G. Liu, Y. Zhang, C. Wang, Q. Li, F. Li, and W. Liu, "A new magnetic target localization method based on two-point magnetic gradient tensor," *Remote Sensing*, vol. 14, no. 23, 2022, ISSN: 2072-4292. DOI: 10.3390/rs14236088. [Online]. Available: https://www.mdpi.com/2072-4292/14/23/6088.

[36] *ARVA-NEOBT PRO User Guide*, Available at https://beaconreviews.com/manuals/ARVA-Neo_BT_Pro_2024-02-07.pdf, ARVA NIC-IMPEX, Feb. 2024.

[37] G. Liu, Y. Zhang, C. Wang, Q. Li, and W. Liu, "Novel magnetic dipole localization method based on normalized source strength," *IEEE Sensors Journal*, vol. 24, no. 16, pp. 26 159–26 170, 2024. DOI: 10.1109/JSEN.2024.3423342.

[38] W. Lv, P. Huang, Y. Yang, Q. Luo, S. Xie, and C. Fu, "A novel method of magnetic sources edge detection based on gradient tensor," *Minerals*, vol. 14, no. 7, 2024, ISSN: 2075-163X. DOI: 10.3390/min14070657. [Online]. Available: https://www.mdpi.com/2075-163X/14/7/657.

Ringraziamenti

SCRIVI QUI I RINGRAZIAMENTI